

Chapter 5

Development of green methodology for the synthesis of reusable metal NPs using agro-waste and its application in oxidative C_{sp^2} - C_{sp^2} and C_{sp^2} - C_{sp} bond forming reaction

This chapter is composed of two sections, the generation of Pd and Cu_2O/Cu NPs using agro-waste extract without the assistance of any external reducing agents and its application in Suzuki-Miyaura and Sonogashira cross-coupling reaction.

Section 5.1

Synthesis of efficient Pd NPs using papaya peel and its implication in Suzuki-Miyaura and Sonogashira cross-coupling reaction.

Abstract: In this section we focus on the utilization of organic waste for synthesis of Pd NPs and investigation of its catalytic activity in Suzuki-Miyaura and Sonogashira cross-coupling reaction. An efficient reusable Pd NPs has been synthesized in a green and environmentally viable route, using the extract of waste papaya peel without the assistance of any conventional strategies.

5.1.1. Introduction

Palladium continues to attract great interest because of its versatility as a catalyst that mediates various C-C bond forming reactions [1,2]. Among them, Suzuki-Miyaura and Sonogashira cross-coupling reactions are reliable and powerful methods for the synthesis of biaryl and acetylenyl derivatives. Consequently, there is a need to design a highly efficient, cost-effective, simple, and commercially viable methodologies for the synthetic purposes. Nowadays, metal nanoparticles (NPs) have received particular interest in a wide range of research fields because of their fabulous ability as a nano catalyst contributing both the homogeneous and heterogeneous characteristics [3]. Conventional methods for synthesis of NPs involve the usage of toxic chemicals, formation of hazardous by-products, and draws contamination from precursor chemicals. In this aspect, environment-friendly green chemistry-based approach such as microorganisms (bacteria, fungi, algae, and yeast) and plants draws significant advantages over the conventional chemical and physical techniques [4,5]. However, the use of plant resources for synthetic application might leads to destruction of ecologically important plants and plant parts. In order to avoid this and to serve the purpose of pollution mitigation, agro waste can be used as alternative sources, which are otherwise a significant source of pollution and creates waste management issues. In general, the processing of various fruits and plant resources in industries or its fresh consumption, results about 20–25% of waste (peels and seeds) which are abundant natural waste materials across the world [6]. So, waste utilization from food processing industries is highly essential and challenging task all around the globe. So, recyclability of the waste by-products in organic synthesis is an encouraging approach as per green chemistry point of view. Recently, various agricultural wastes such as fruit peels and their extracts were widely used for the production of cellulose nanofibers and for various research applications [7,8]. Considering this aspects, we have synthesized Pd NPs in an eco-friendly manner by using the water extract of fresh peel of papaya fruits at room temperature without using any reducing agent. The catalytic activity of the synthesized Pd NPs was investigated in oxidative $C_{sp^2}-C_{sp^2}$ and $C_{sp^2}-C_{sp}$ bond forming reaction. The formation of Pd NPs and its structural and morphological characteristics are examined by UV-visible spectroscopy, X-ray diffraction, Transmission electron microscopy (TEM), Scanning electron microscopy (SEM), Energy-dispersive X-ray Spectroscopy (EDX) and BET analysis.

5.1.2. Experimental

5.1.2.1. General procedure for preparation of Pd NPs

10 g papaya peel was washed with distilled water, finely chopped and then grinded with 100 mL distilled water. The extract was filtered through sintered glass crucible. In a 5 mL round bottom flask 2 mL of the aqueous extract was mixed with 0.1 g Pd(OAc)₂ and stirred for 48 hours at room temperature under nitrogen atmosphere (Figure 5.1.1). The resulting Pd NPs were separated through centrifugation and the black products were dried under vacuum.

5.1.2.2. Experimental procedure for the catalytic reactions

(A) Typical procedure for Suzuki-Miyaura reaction of aryl halides using Pd NPs: Aryl halide (0.5 mmol), aryl boronic acid (0.6 mmol), K₂CO₃ (1.5 mmol), catalyst (0.0009 mmol) and 4 mL solvent were taken in a 25 mL round-bottom flask. The reactants were stirred at room temperature for the required time. After completion, (vide TLC) the catalyst was separated from the reaction mixture by centrifugation and the crude reaction mixture was extracted with ethyl acetate (3×10 mL). The resultant organic phases was washed with brine (2×10 mL) and dried over anhydrous Na₂SO₄, filtered and evaporated under reduced pressure and purified by column chromatography using ethyl acetate and n-hexane as eluent. The products were characterized by ¹H and ¹³C NMR spectroscopic analyses.

For recycling experiments, the reaction mixture was centrifuged and the residue catalyst was washed four times with excess water and then with ethyl acetate in sequence. The resultant catalyst was dried under vacuum and subjected to consequent run.

(B) Typical procedure for Sonogashira cross-coupling reactions using Pd NPs: Aryl halide (1 mmol), terminal acetylene (1.5 mmol), base (1.5 mmol), catalyst (0.02 mmol) and ethanol (3 mL) were taken in a 25 mL round-bottom flask. The reactants were stirred at 60 °C under aerobic condition. After completion (vide TLC) the catalyst was separated from the reaction mixture by centrifugation and the crude reaction mixture was extracted with ethyl acetate (3×10 mL) and dried over anhydrous Na₂SO₄. The products were purified by column chromatography using n-hexane and ethyl acetate as eluent. The products were identified by ¹H and ¹³C NMR spectroscopic analyses.

For recycling experiments of Sonogashira reaction, similar procedure was followed like Suzuki-Miyaura cross-coupling reaction.

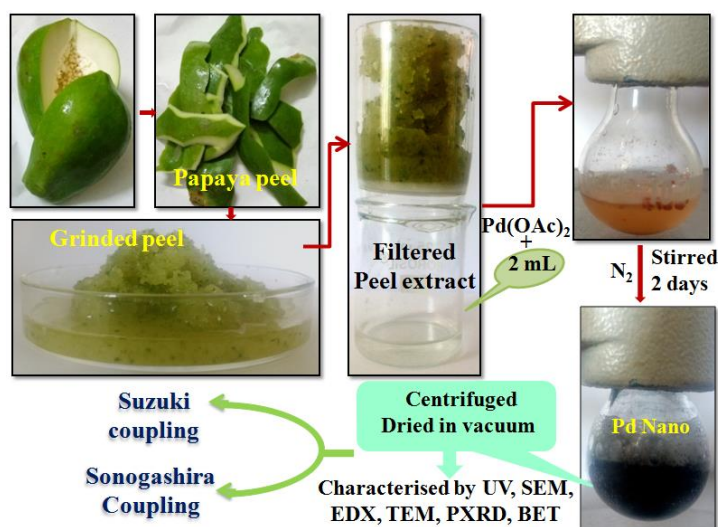


Figure 5.1.1: Preparation of Pd NPs from waste papaya peels.

5.1.3. Results and Discussion

5.1.3.1. Characterizations of Pd NPs

The Pd NP was synthesised by direct mixing of Pd(OAc)₂ with aqueous extract of papaya peel at room temperature. After 2 days, the colour of the reaction mixture became black from brown which indicates the formation of Pd NPs. Figure 5.1.1 shows the change in colour during reduction of Pd(II) to Pd(0) NPs. The Flavin Mono Nucleotide (FMN) and flavin adenine dinucleotide (FAD) present in papaya peel may act as a reductant for reduction of Pd(OAc)₂ [9]. However in order to confirm the formation of Pd NPs and to understand its structural and morphological characteristics various analytical studies have been done.

Initially, UV/Vis absorption spectroscopy has been performed which shows a prominent band at 269 nm of the papaya peel extract (Figure 5.1.2a). Again, the absorption bands of Pd(OAc)₂ solution above 270 nm were assigned for LMCT transition [10,11]. Addition of papaya peel extract into Pd(II) solution shows a distinctive overlapping peak approximately in the same region as that of the extract (Figure 5.1.2b). The absorption spectrum of the suspension of Pd NPs after bio-reduction results in the appearance of a new broad peak which confirms the formation of Pd(0) particles (Figure 5.1.2c).

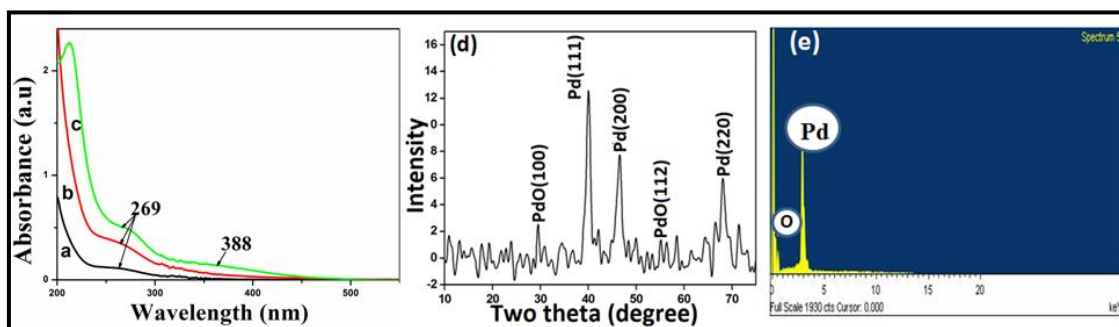


Figure 5.1.2: (a, b & c) are UV/Vis absorption spectra of papaya extract, mixture of papaya extract & Pd(OAc)₂ and Pd NPs respectively (d) Powder XRD pattern of Pd NPs (e) EDX analysis of Pd NPs.

Powder XRD pattern of Pd NPs shows the formation of face centered cubic (fcc) lattices system of palladium nanostructure (JCPDS Card No. 89-4897) (Figure 5.1.2d). The observed peaks of Pd at $2\theta = 39.9, 46.4$ and 67.1 degree corresponds to (111), (200) and (220) reflections respectively along with two additional diffraction peaks of PdO (JCPDS card No. 75-0200) at $2\theta = 39.5$ and 46.4° for (111) and (200) reflections. This was further confirmed by EDX analysis which reveals the presence of Pd and O (Figure 5.1.2e). The Pd(0) initially formed might have transformed to PdO via aerial oxidation as reported in literature [12].

Next, the morphology and surface structure of Pd NPs were analysed by electron microscopic studies. From the TEM images, it is seen that Pd NPs are spherical and crystalline in nature with particle sizes ranging between 1-5 nm (Figure 5.1.3a). The distribution of the synthesised Pd NPs was analyzed using Gaussian fits and presented in the form of histogram, showing 80% of the Pd NPs size fall in 1-3 nm with mean size 2.4 nm (Figure 5.1.3b). Again, (Figure 5.1.3 c & d) confirm the presence of crystal planes with the lattice spacing of 0.22 nm and 0.19 nm which is consistent with inter planer spacing (111) and (200) lattice planes of face centre cubic (fcc) Pd NPs. The corresponding SAED pattern of Pd NPs represents four well-resolved rings corresponding to crystallographic planes (111), (200), (220) and (311) of Pd NPs (Figure 5.1.3c). These results are consistent with the powder XRD data and matches well with d-values obtained from standard JCPDS database.

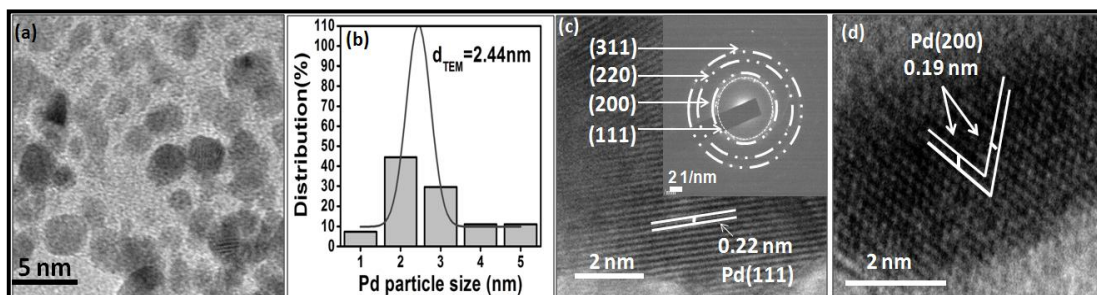


Figure 5.1.3: (a) TEM image, (b) Pd NPs distribution and (c) & (d) HRTEM images of Pd NPs.

Again the SEM images presented in Figure 5.1.4 a & b, show the porosity of the Pd NPs. This was further confirmed by BET surface analysis method (Figure 5.1.4 c). The N_2 adsorption/desorption isotherm shown in Figure 5.1.4c of Pd NPs belongs to Type IV with H3 hysteresis loop with upper closure point $P/P_0 \geq 0.9$ which are demarcated as a characteristic of mesoporous material. Additionally, the specific surface area as calculated by the BET equation was about $18.2 \text{ m}^2/\text{g}$ and pore diameter 3.7 nm . Moreover, the pore size distribution curve (inset) also indicates the mesoporosity of the Pd NPs (Figure 5.1.4d).

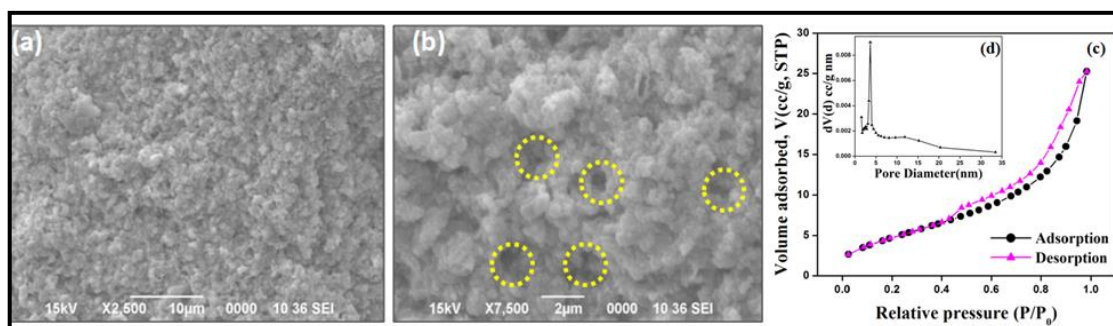


Figure 5.1.4: (a) & (b) SEM images, (c) BET surface area and inset, (d) pore size distribution of Pd NPs.

5.1.3.2. Catalytic activity of Pd NP

5.1.3.2.1. Optimization of catalytic system for Suzuki-Miyaura coupling reaction

The efficiency of the catalytic system is initially assessed in Suzuki-Miyaura cross-coupling reaction of 4-bromoanisole and phenylboronic acid with 0.001 mmol Pd NP using different bases in H_2O at room temperature (Table 5.1.1). Among the different bases studied, K_2CO_3 was found to be the most effective in terms of reaction efficiency and time (Table 5.1.1, entries 1-7). We have also performed the reaction in different

solvent systems such as EtOH, *i*-PrOH, CH₃CN and H₂O: EtOH (1:1) (Table 5.1.1, entries 9-13). Interestingly, H₂O: EtOH (1:1) system delivers the desired product within shorter reaction time (Table 5.1.1, entry 13). Again, the reaction was examined by lowering the amount of Pd catalyst. It can be seen that, 95% yield of the cross-coupling product was achieved using 0.0009 mmol of Pd NP (Table 1, entries 12 and 13). However, the reaction did not proceed in absence of catalyst (Table 5.1.1, entry 14).

Table 5.1.1: Optimization of the amount of catalyst and base for Suzuki-Miyaura coupling reaction ^[a]

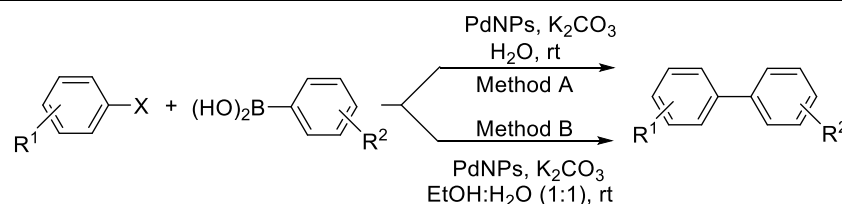
MeO-C₆H₄-Br + (HO)₂B-C₆H₅ $\xrightarrow[\text{H}_2\text{O, rt}]{\text{PdNPs, Base}}$ MeO-C₆H₄-C₆H₅

Entry	PdNPs (mmol)	Base (mmol)	Solvent (mL)	Time (h)	Yield (%) ^[b]
1	0.001	K ₂ CO ₃	H ₂ O	2	95
2	0.001	Na ₂ CO ₃	H ₂ O	2	95
3	0.001	Cs ₂ CO ₃	H ₂ O	2	95
4	0.001	Na ₃ PO ₄ ·12H ₂ O	H ₂ O	2	90
5	0.001	NaOH	H ₂ O	3	60
6	0.001	KOH	H ₂ O	3	65
7	0.001	Et ₃ N	H ₂ O	3	40
8	0.001	-	H ₂ O	12	-
9	0.001	K ₂ CO ₃	EtOH	8	70
10	0.001	K ₂ CO ₃	<i>i</i> -PrOH	8	80
11	0.001	K ₂ CO ₃	CH ₃ CN	8	70
12	0.0009	K ₂ CO ₃	H ₂ O	2	95
13	0.0009	K ₂ CO ₃	H ₂ O:EtOH (1:1)	30 min	95
14	-	K ₂ CO ₃	H ₂ O:EtOH (1:1)	12	-

^[a]Reaction conditions: 4-bromoanisole (0.5 mmol), phenylboronic acid (0.6 mmol), base (1.5 mmol), rt (25 °C) in air unless otherwise noted. ^[b] Isolated yields

5.1.3.2.2. Substrate scope for Suzuki-Miyaura coupling reaction

From the optimization table (Table 5.1.1), it is seen that, similar yield was achieved using H₂O and H₂O: EtOH (1:1) as the reaction medium. Literature studies revealed that only few reports are available with excellent efficiencies using pure water as a solvent [13]. The insolubility of most of the substrates in water sometimes delays the reaction process. So, considering the optimization conditions as discussed in Table 5.1.1, we have performed a comparative study for electronically diverse aryl bromides and aryl boronic acids using both in distilled water (Method A) and 1:1 ratio of H₂O and EtOH (Method B), (Table 5.1.2).

Table 5.1.2: Substrate scope for Pd NPs catalyzed Suzuki-Miyaura reaction ^[a]


Entry	X	R ¹	R ²	Method A		Method B	
				Time(h)	Yield (%) ^[c]	Time(min)	Yield (%) ^[c]
1	Br	H	H	1	98	15	98
2	Br	H	OCH ₃	1	95	15	98
3	Br	H	Cl	3	95	20	98
4	Br	4-OCH ₃	H	2	95	30	95
5	Br	4-OCH ₃	OCH ₃	1	95	30	95
6	Br	4-OCH ₃	Cl	1	90	30	95
7	Br	4-OCH ₃	3-CH ₃	2	90	30	95
8	Br	2-OCH ₃	H	8	80	60	80
9	Br	4-CH ₃	H	2	95	20	98
10	Br	4-CH ₃	OCH ₃	2	95	20	98
11	Br	4-CH ₃	<i>t</i> -Bu	2	95	20	96
12	Br	4-CH ₃	Cl	3	92	20	98
13	Br	4-NO ₂	<i>t</i> -Bu	8	95	20	96
14	Br	4-NO ₂	H	7, (2) ^[b]	98, (98) ^[b]	20	98
15	Br	4-NO ₂	OCH ₃	8, (2) ^[b]	90, (92) ^[b]	20	95
16	Br	4-NO ₂	Cl	8	50	20	98
17	Br	4-CHO	H	8	90	30	98
18	Br	4-CHO	OCH ₃	8	85	30	95
19	Br	4-CHO	Cl	8	50	30	96
20	Br	4-COMe	H	12	60	20	95
21	Br	4-COMe	OCH ₃	12	50	30	92
22	Br	4-COMe	Cl	12	50	30	95
23	Cl	4-OCH ₃	H	12	20	12	50 ^[b]
24	Cl	4-CH ₃	H	12	40	12	50 ^[b]
25	Cl	4-OCH ₃	H	24	20 ^[d]	24	nr ^[e]

^[a] Reaction Conditions: aryl bromide (1 mmol), aryl boronic acid (1.2 mmol), Pd NPs (0.0009 mmol), K₂CO₃ (2 mmol), water (4 mL), rt, ^[b] 80°C in air, ^[c] Isolated yield, ^[d] 90°C, in DMF, ^[e] reflux in CH₃CN

The reactions of electron rich aryl bromides are more efficient than (Table 5.1.2, entries 4-7 and 9-12) electron poor aryl bromides. (Table 5.1.2, entries 13-22). Nitro, formyl & acetyl substituent aryl bromides require extended reaction time in distilled water. Insolubility of these substrates in water may delay the reaction process which can be overcome by using H₂O: EtOH (1:1) as reaction medium (Table 5.1.2, entries 16, 19-

22). As an additional assessment, we have carried out the reaction at high temperature (80°C) using Method A. Similar cross-coupling yield was observed but proceeds in a shorter reaction time (Table 5.1.2, entries 14 and 15). Again, 2-methoxybromobenzene on account of its steric hindrance affects the C-X activation and affords significant low yield even with longer reaction time (Table 5.1.2, entries 4 vs 8). It can be observed that there are no such significant differences in yield and duration for diverse range of aryl boronic acids.

We have also tried to extend the scope of the Pd NPs for aryl chlorides under different reaction conditions, however, no appreciable conversion was noticed even after prolonged reaction time and higher temperature (Table 5.1.2, entries 23-25).

5.1.3.2.3. Optimization of catalytic system for Sonogashira coupling reaction

Next the effectiveness of the synthesized Pd NP was examined in Sonogashira cross-coupling reaction. Initial investigation was done using 4-iodonitrobenzene and phenylacetylene as the model substrate and was standardized by varying the catalyst amount, temperature and different bases and solvents (Table 5.1.3). At first, we were able to isolate very little amount of cross-coupling product using water as the reaction medium even with higher catalyst loading (Table 5.1.3, entries 1 and 2). However use of alcoholic solvents such as EtOH and *i*-PrOH gave better result (Table 5.1.3, entries 3, 4). Using H₂O as co-solvent (EtOH/H₂O 1:1) we obtained a reduced amount of the cross coupled product (Table 5.1.3, entry 5). Other solvents such as toluene, dioxane, THF and DME did not show any positive impact (Table 5.1.3, entries 6-8). The catalyst showed best performance in ethanol at 60 °C (Table 5.1.3, entry 9). The impact of different bases was also examined in ethanol at 60 °C. Hydroxide bases such as NaOH and KOH and organic base Et₃N were found to be less effective (Table 5.1.3, entries 13-15). In contrast, carbonate such as Na₂CO₃, K₂CO₃ and Cs₂CO₃ provide excellent cross-coupling yield (Table 5.1.3, entries 9-11). Next by varying the catalyst loading we found that 0.02 mmol Pd NPs was sufficient for the coupling reaction (Table 5.1.3, entry 16). On further decreasing the amount of catalyst, lower yield of diarylalkyne was obtained (Table 5.1.3, entry 17).

Table 5.1.3: Optimization of catalyst and Solvent in Sonogashira cross-coupling reaction

[a]

Entry	Catalyst (mmol)	Base (mmol)	Solvent (mL)	Temperature (°C)	Time (h)	Yield (%) ^[b]
1	0.001	K ₂ CO ₃	Water	25	12	20
2	0.03	K ₂ CO ₃	Water	25	12	40
3	0.03	K ₂ CO ₃	<i>i</i> -PrOH	25	12	60
4	0.03	K ₂ CO ₃	EtOH	25	12	60
5	0.03	K ₂ CO ₃	EtOH/H ₂ O(1:1)	25	12	40
6	0.03	K ₂ CO ₃	Dioxane	25	12	30
7	0.03	K ₂ CO ₃	THF	25	12	35
8	0.03	K ₂ CO ₃	DME	25	12	35
9	0.03	K ₂ CO ₃	EtOH	60	4	98
10	0.03	Na ₂ CO ₃	EtOH	60	5	98
11	0.03	CS ₂ CO ₃	EtOH	60	4	98
12	0.03	Na ₃ PO ₄ ·12H ₂ O	EtOH	60	5	90
13	0.03	NaOH	EtOH	60	12	70
14	0.03	KOH	EtOH	60	12	70
15	0.03	NEt ₃	EtOH	60	12	40
16	0.02	K ₂ CO ₃	EtOH	60	4	98
17	0.01	K ₂ CO ₃	EtOH	60	12	70

^[a] Reaction conditions: 4-iodonitrobenzene (0.5 mmol), phenylacetylene (0.75 mmol), Solvent (4 mL), base (1.5 mmol); ^[b] Isolated yields.

5.1.3.2.4. Substrate scope for Sonogashira coupling reaction

Coupling of electronically diverse aryl halides and terminal alkynes were studied considering this optimized reaction conditions (Table 5.1.4). Iodobenzene reacts with terminal alkynes, delivering good to excellent yields of the products (Table 5.1.4, entries 1-4). Even less reactive substrates like 1-hexyne gave excellent yield of the product (Table 5.1.4, entry 3). Additionally, both electron poor and electron rich *p*-substituted aryl iodides afforded the coupling products in excellent yields (Table 5.1.4 entries 5, 8 and 10). However, it is observed that with 4-iodotoluene the reaction completed within shorter reaction time compared to 4-iodonitrobenzene (Table 5.1.4, entry 5 vs 8). Similar results were observed with *meta* substituted aryl iodides (Table 5.1.4, entries 6 and 9), with 3-iodotoluene being more competent than 3-iodonitrobenzene. But, a steric effect as in 2-iodonitrobenzene relatively lowered the reaction yield (Table 5.1.4, entry 7).

Notably, coupling of electron donating 4-iodoanisole and 4-iodoaniline with phenylacetylene give slightly lower yields (Table 5.1.4, entries 13 and 14).

Table 5.1.4: Pd NPs catalyzed Sonogashira cross-coupling reaction of aryl halides with terminal alkyne ^[a]

Entry	R ¹	R ²	X	Time (h)	Yield (%) ^[c]
1	H	C ₆ H ₅	I	5	98
2	H	Dodecyl	I	8	85
3	H	Hexyl	I	4	95
4	H	Cyclohexyl	I	5	90
5	4-NO ₂	C ₆ H ₅	I	4	98
6	3-NO ₂	C ₆ H ₅	I	6	85
7	2-NO ₂	C ₆ H ₅	I	8	40
8	4-CH ₃	C ₆ H ₅	I	1	98
9	3-CH ₃	C ₆ H ₅	I	6	90
10	4-CH ₃	4-CH ₃ C ₆ H ₅	I	2	96
11	4-CH ₃	Hexyne	I	8	80
12	4-CH ₃	Cyclohexyl	I	8	85
13	4-OCH ₃	C ₆ H ₅	I	8	70
14	4-NH ₂	C ₆ H ₅	I	8	50
15	H	C ₆ H ₅	Br	8	90 ^[b]
16	4-CH ₃	4-CH ₃ C ₆ H ₅	Br	8	75 ^[b]
17	4-CH ₃	C ₆ H ₅	Br	8	85 ^[b]
18	4-NO ₂	C ₆ H ₅	Br	8	60 ^[b]

^[a] Reaction conditions: aryl halide (0.5 mmol), terminal alkyne (1 mmol), Pd NPs (0.02 mmol), EtOH (4 mL), base (1.5 mmol); ^[b] reaction done at 80 °C. ^[c] Isolated yields.

Next, the effectiveness of this catalytic system was examined for electronically varied aromatic and aliphatic alkynes (Table 5.1.4, entries 2-4, and 10-12). Comparable yield was isolated with phenyl acetylene and *p*-tolylphenylacetylene (Table 5.1.4, entry 10). Moderate yields were obtained when aliphatic alkynes were used as coupling partners. However, iodobenzene shows better reactivity with range of aliphatic alkynes (Table 5.1.4, entries 2-4). Again, in the reaction between aryl bromides and terminal acetylene, very low product formation was observed. Hence, we have performed the reaction at 80 °C keeping the other parameters same (Table 5.1.4, entry 15). It was observed that electron rich aryl bromide gave better result (Table 5.1.4, entries 16 and 17) compared to electron poor aryl bromide, rendering only 60% isolated yield in case of 4-iodonitrobenzene (Table 5.1.4, entry 18). A comparison of the effectiveness of the

current Pd(0) NP and some reported catalysts for Suzuki and Sonogashira cross-coupling reactions is listed in Table 5.1.5. The present catalyst has the advantage of milder reaction conditions, aqueous solvent, ligand- and additive-free conditions, and use of natural feedstock.

Table 5.1.5: Comparison of the present protocol with some existing literatures

Entry	Catalyst	Reaction	Reaction condition	Yield (%)
1 [14]	<i>in situ</i> PdNPs formed from Pd(II) complexes of chalcogenated Schiff bases	Suzuki Coupling	DMF:H ₂ O(3:1), K ₂ CO ₃ , 90°C, 2-12h	62-98
		Sonogashira Coupling	DMF, K ₂ CO ₃ , 90-110°C, 1-24h	56-99
2 [15]	Pd(II) Acyclic Diaminocarbene Complexes@Polystyrene	Suzuki Coupling	DMF:H ₂ O, Et ₃ N/K ₂ CO ₃ , 65-70°C, 1-2h	65-98
		Sonogashira Coupling	DMF, Et ₃ N, CuI, 16-70°C, 5-180min	93-99
3 [16]	SiO ₂ @Fe ₃ O ₄ -Pd	Suzuki Coupling	K ₂ PO ₄ , MeOH, 60-110°C, 1.5-10h	26-99
		Sonogashira Coupling	DMF, K ₂ CO ₃ , 100°C, 6h	71-97
4	PdNPs (Our Work)	Suzuki Coupling	H ₂ O, K ₂ CO ₃ , rt, 3-12h	88-98
			50% aq.EtOH, K ₂ CO ₃ , rt, 15-30 min	92-98
		Sonogashira Coupling	EtOH, K ₂ CO ₃ , 60°C, 4-8h	40-98

5.1.3.2.5. Catalyst reusability

The recyclability of a catalyst is an important aspect from the green chemistry point of view. The recycling test was done for both Suzuki-Miyaura and Sonogashira coupling reaction considering the optimization substrates (Figure 5.1.5). After the fresh catalytic run, the reaction mixture was subjected to centrifugation. The filtrate was separated and extracted with ethyl acetate for isolation of pure product and the residue catalyst was washed with excess water and ethyl acetate in sequence which is then dried under vacuum and used for next consecutive run with the addition of fresh reactants. We have observed that the catalyst can be reused up to four cycles for both the cross-coupling reactions without much loss in its catalytic activity.

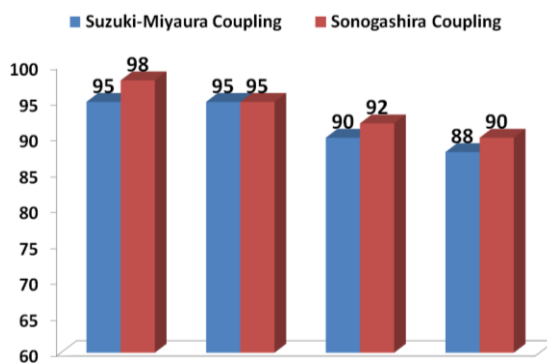
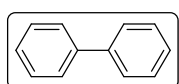


Figure 5.1.5: Reusability of Pd NPs for the coupling reactions

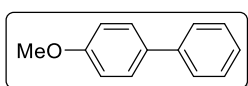
5.1.4. Conclusions

This section provides a green and economical alternative strategy for the synthesis of biaryls and acetylenyl derivatives under an aerobic atmosphere without the need for any ligand assisting system. The Pd NPs has been synthesized from inexpensive starting materials without using any reducing and capping reagent in water at room temperature. The current method prioritizes the utilization of waste and is associated with minimizing hazards, risk, energy and cost related to synthetic procedures.

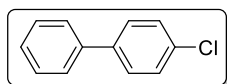
5.1.5. Analytical data of the synthesized biaryl and alkynyl derivatives



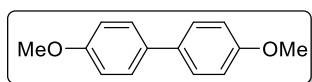
Biphenyl: (Table 5.1.2, entry 1): White Solid, m.p. 69-70 °C, ^1H NMR (400 MHz, CDCl_3): δ 7.60-7.58 (m, 4H), 7.46-7.41 (m, 4H), 7.36-7.32 (m, 2H) ppm. ^{13}C NMR (100 MHz, CDCl_3): δ 141.3, 128.8, 127.3, 127.2 ppm.



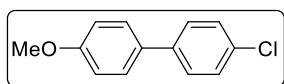
4-Methoxybiphenyl: (Table 5.1.2, entry 4): White Solid, m.p. 81-83 °C, ^1H NMR (400 MHz, CDCl_3): δ 7.58-7.49 (m, 4H), 7.44-7.38 (m, 2H), 7.31 (dt, 1H, $J = 9.1, 4.3$ Hz), 7.01-6.94 (m, 2H), 3.85 (s, 3H) ppm. ^{13}C NMR (100 MHz, CDCl_3): δ 159.2, 140.9, 133.8, 128.8, 128.2, 126.8, 126.7, 114.2, 55.4 ppm.



4-Chlorobiphenyl: (Table 5.1.2, entry 3): White Solid, m.p. 77-79 °C, ^1H NMR (400 MHz, CDCl_3): δ 7.56-7.33 (m, 9H) ppm. ^{13}C NMR (100 MHz, CDCl_3): δ 134.6, 132.8, 132.0, 129.3, 128.6, 128.5, 128.3, 124.7 ppm.

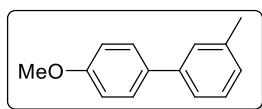


4, 4'-Dimethoxybiphenyl: (Table 5.1.2, entry 5): Yellow Solid, m.p. 179-181 °C, ^1H NMR (400 MHz, CDCl_3): δ 7.53-7.28 (m, 4H), 7.06-6.77 (m, 4H), 3.83 (s, 6H) ppm. ^{13}C NMR (100 MHz, CDCl_3): δ 158.7, 133.5, 127.8, 114.2, 55.4 ppm.



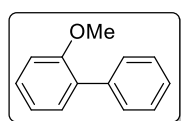
4-Chloro-4'-methoxybiphenyl: (Table 5.1.2, entry 6): White

Solid, m.p. 104-106 °C, $^1\text{H NMR}$ (400 MHz, CDCl_3): δ 7.48-7.44 (m, 4H), 7.36 (d, 2H, $J = 8.7$ Hz), 6.97 (d, 2H, $J = 8.2$ Hz), 3.85 (s, 3H) ppm. $^{13}\text{C NMR}$ (100 MHz, CDCl_3): δ 159.4, 149.7, 139.3, 132.7, 132.5, 128.9, 128.1, 114.3, 55.4 ppm.



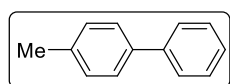
4-Methoxy-3'-methylbiphenyl: (Table 5.1.2, entry 7): White

Solid, m.p. 48-49 °C, $^1\text{H NMR}$ (400 MHz, CDCl_3): δ 7.59-7.48 (m, 2H), 7.35 (ddd, 3H, $J = 16.3, 7.9, 0.7$ Hz), 7.18-7.11 (m, 1H), 7.03-6.91 (m, 2H), 3.85 (s, 3H), 2.43 (s, 3H).ppm. $^{13}\text{C NMR}$ (100 MHz, CDCl_3): δ 159.1, 140.9, 138.3, 133.9, 128.7, 128.2, 127.6, 127.5, 123.9, 114.2, 55.4, 21.6 ppm.



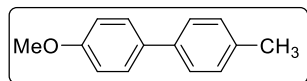
2-Methoxybiphenyl: (Table 5.1.2, entry 8): Colourless liquid, $^1\text{H NMR}$

(400 MHz, CDCl_3): δ 7.59-7.50 (m, 2H), 7.47-7.39 (m, 2H), 7.38-7.29 (m, 3H), 7.10-6.95 (m, 2H), 3.82 (s, 3H) ppm. $^{13}\text{C NMR}$ (100 MHz, CDCl_3): δ 156.5, 140.9, 138.6, 131.0, 129.6, 128.7, 128.0, 127.0, 120.9, 111.3, 55.6 ppm.



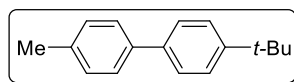
4-Methylbiphenyl: (Table 5.1.2, entry 9): White Solid, m.p. 46-48

°C, $^1\text{H NMR}$ (400 MHz, CDCl_3): δ 7.59 (dd, 2H, $J = 8.3, 1.2$ Hz), 7.54-7.48 (m, 2H), 7.47-7.39 (m, 2H), 7.37-7.22 (m, 3H), 2.41 (s, 3H).ppm. $^{13}\text{C NMR}$ (100 MHz, CDCl_3): δ 141.2, 138.4, 137.1, 129.5, 128.8, 127.3, 127.2, 127.0, 21.1 ppm.



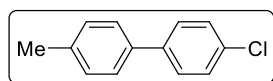
4-Methyl-4'-methoxybiphenyl: (Table 5.1.2, entry 10):

White Solid, m.p. 102-104°C, $^1\text{H NMR}$ (400 MHz, CDCl_3): δ 7.53-7.47 (m, 2H), 7.44 (d, 2H, $J = 8.1$ Hz), 7.24-7.19 (m, 2H), 6.99-6.92 (m, 2H), 3.84 (s, 3H), 2.37 (s, 3H) ppm. $^{13}\text{C NMR}$ (100 MHz, CDCl_3): δ 159.0, 138.0, 136.4, 133.8, 129.5, 128.0, 126.6, 114.2, 55.4, 21.1 ppm.



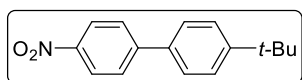
4-Methyl-4'-t-butylbiphenyl: (Table 5.1.2, entry 11): White

Solid, m.p. 120-124 °C, $^1\text{H NMR}$ (400 MHz, CDCl_3): 7.55-7.45 (m, 6H), 7.25-7.24 (m, 2H), 2.40 (s, 3H), 1.37 (s, 9H) ppm. $^{13}\text{C NMR}$ (100 MHz, CDCl_3): δ 150.0, 138.3, 136.8, 129.5, 127.1, 126.9, 126.7, 125.7, 34.6, 31.4, 21.2 ppm.



4-Chloro-4'-methylbiphenyl: (Table 5.1.2, entry 12): White

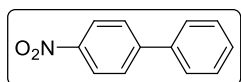
Solid, m.p. 122-124 °C, $^1\text{H NMR}$ (400 MHz, CDCl_3): 7.50-7.48 (m, 2H), 7.45-7.43 (m, 2H), 7.41-7.36 (m, 2H), 7.25-7.23(m, 2H), 2.38 (s, 3H) ppm. $^{13}\text{C NMR}$ (100 MHz, CDCl_3): δ 139.6, 137.5, 137.1, 133.1, 129.6, 129.1, 128.9, 128.2, 21.2 ppm.



4-Nitro-4'-t-butylbiphenyl: (Table 5.1.2, entry 13): Pale yellow Solid, m.p. 110-112 °C, $^1\text{H NMR}$ (400 MHz, CDCl_3):

8.27 (d, 2H, $J = 8.7$ Hz), 7.72 (d, 2H, $J = 8.7$ Hz), 7.58-7.49 (m, 4H), 1.36 (s, 9H) ppm.

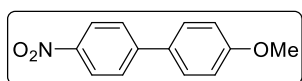
$^{13}\text{C NMR}$ (100 MHz, CDCl_3): δ 152.3, 147.5, 135.8, 132.5, 127.6, 127.1, 126.2, 124.2, 34.8, 31.3 ppm.



4-Nitrobiphenyl: (Table 5.1.2, entry 14): Yellow Solid, m.p. 113-115 °C, $^1\text{H NMR}$ (400 MHz, CDCl_3): δ 8.34-8.24 (m, 2H), 7.79-

7.68 (m, 2H), 7.65-7.59 (m, 2H), 7.48 (ddd, $J = 14.5, 10.4, 6.7$ Hz, 3H) ppm. $^{13}\text{C NMR}$

(100 MHz, CDCl_3): δ 147.7, 138.8, 129.2, 128.9, 127.9, 127.4, 124.2, 120.0 ppm.

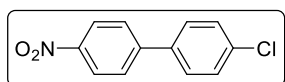


4-Methoxy-4'-nitrobiphenyl: (Table 5.1.2, entry 15): Yellow Solid, m.p. 97-99 °C, $^1\text{H NMR}$ (400 MHz, CDCl_3): δ 8.26 (d,

2H, $J = 8.9$ Hz), 7.68 (d, 2H, $J = 8.9$ Hz), 7.57 (d, 2H, $J = 8.9$ Hz), 7.01 (d, 2H, $J = 8.8$

Hz), 3.86 (s, 3H) ppm. $^{13}\text{C NMR}$ (100 MHz, CDCl_3): δ 160.5, 147.3, 146.6, 131.1,

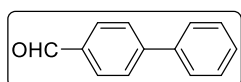
128.6, 127.1, 124.2, 114.6, 55.5 ppm.



4-Chloro-4'-nitrobiphenyl: (Table 5.1.2, entry 16): Pale Yellow Solid, m.p. 142-145 °C, $^1\text{H NMR}$ (400 MHz, CDCl_3): δ

8.30-8.27 (m, 2H), 7.70-7.68 (m, 2H), 7.55-8.53 (m, 2H), 7.47-7.44 (m, 2H) ppm. ^{13}C

NMR (100 MHz, CDCl_3): δ 146.4, 137.2, 135.3, 129.4, 129.0, 128.7, 127.7, 124.3 ppm.

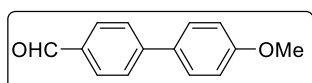


4-Formylbiphenyl: (Table 5.1.2, entry 17): White Solid, m.p. 57-59 °C, $^1\text{H NMR}$ (400 MHz, CDCl_3): δ 10.05 (s, 1H), 7.95 (d, 2H, J

$= 8.2$ Hz), 7.74 (d, 2H, $J = 8.2$ Hz), 7.64-7.62 (m, 2H), 7.49-7.39 (m, 3H) ppm. ^{13}C

NMR (100 MHz, CDCl_3): δ 192.0, 147.3, 139.8, 135.2, 130.3, 129.1, 128.5, 127.7,

127.4 ppm.



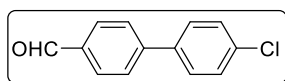
4-Formyl-4'-methoxybiphenyl: (Table 5.1.2, entry 18):

White Solid, m.p. 100-101°C, $^1\text{H NMR}$ (400 MHz, CDCl_3): δ

10.02 (s, 1H), 7.91 (dd, 2H, $J = 4.9, 3.5$ Hz), 7.70 (dd, 2H, $J = 4.6, 3.7$ Hz), 7.63-7.52

(m, 2H), 7.05-6.90 (m, 2H), 3.86 (s, 3H) ppm. $^{13}\text{C NMR}$ (100 MHz, CDCl_3): δ 191.9,

160.2, 146.8, 134.7, 132.1, 130.4, 128.5, 127.1, 114.5, 55.4 ppm.

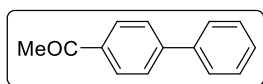


4-Formyl-4'-chlorobiphenyl: (Table 5.1.2, entry 19): White Solid, m.p. 114-118 °C, $^1\text{H NMR}$ (400 MHz, CDCl_3): δ 10.05

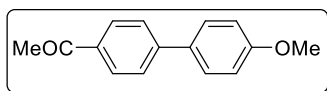
(s, 1H), 7.99-7.87 (m, 2H), 7.74-7.66 (m, 2H), 7.59-7.49 (m, 2H), 7.49-7.38 (m,

2H).ppm. $^{13}\text{C NMR}$ (100 MHz, CDCl_3): δ 191.9, 145.9, 138.2, 135.4, 134.8, 130.4,

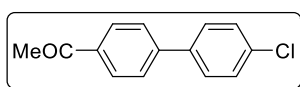
129.1, 128.7, 127.6 ppm.



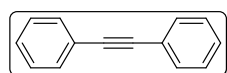
4-Acetylbiphenyl: (Table 5.1.2, entry 20): White Solid, m.p. 118-120 °C, $^1\text{H NMR}$ (400 MHz, CDCl_3): δ 8.03 (d, 2H, $J = 8.2$ Hz), 7.68 (d, 2H, $J = 8.3$ Hz), 7.65-7.59 (m, 2H), 7.46 (t, 2H, $J = 7.6$ Hz), 7.42-7.36 (m, 1H), 2.63 (s, 3H) ppm. $^{13}\text{C NMR}$ (100 MHz, CDCl_3): δ 197.9, 145.8, 139.9, 135.9, 129.0, 128.8, 128.3, 127.3, 127.1, 26.7 ppm.



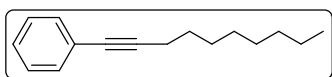
4-Acetyl-4'-methoxybiphenyl: (Table 5.1.2, entry 21): White Solid, m.p. 149-151°C, $^1\text{H NMR}$ (400 MHz, CDCl_3): δ 8.00 (d, 2H, $J = 8.4$ Hz), 7.63 (d, 2H, $J = 8.4$ Hz), 7.57 (d, 2H, $J = 8.7$ Hz), 6.99 (d, 2H, $J = 8.8$ Hz), 3.85 (s, 3H), 2.62 (s, 3H).ppm. $^{13}\text{C NMR}$ (100 MHz, CDCl_3): δ 197.8, 159.9, 145.4, 135.3, 132.3, 129.0, 128.4, 126.7, 114.4, 55.4, 26.7 ppm.



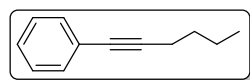
4-Acetyl-4'-chlorobiphenyl: (Table 5.1.2, entry 22): White Solid, m.p. 104-106 °C, $^1\text{H NMR}$ (400 MHz, CDCl_3): δ 8.02 (d, 2H, $J = 8.7$ Hz), 7.64 (d, 2H, $J = 8.6$ Hz), 7.54 (d, 2H, $J = 8.7$ Hz), 7.43 (d, 2H, $J = 8.7$ Hz), 2.63 (s, 3H) ppm. $^{13}\text{C NMR}$ (100 MHz, CDCl_3): δ 197.7, 144.5, 138.3, 136.1, 134.5, 129.2, 129.1, 128.5, 127.1, 26.8 ppm.



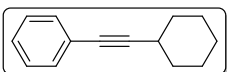
Diphenylacetylene (Table 5.1.4, entry 1): White Solid, m.p. 54-56 °C, $^1\text{H NMR}$ (400 MHz, CDCl_3): δ 7.54-7.52 (m, 4H), 7.34-7.32 (m, 6H) ppm. $^{13}\text{C NMR}$ (100 MHz, CDCl_3): δ 131.7, 128.4, 128.3, 123.3, 89.5 ppm



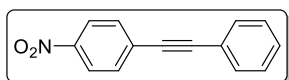
1-(Dodec-1-yn-1-yl)-benzene (Table 5.1.4, entry 2): yellow liquid; $^1\text{H NMR}$ (400 MHz, CDCl_3): δ 7.40-7.37 (m, 2H), 7.27-7.25 (m, 3H), 2.39 (t, 2H, $J = 6.8$ Hz), 1.62-1.27 (m, 12H), 0.88 (t, 3H, $J = 6.8$ Hz) ppm. $^{13}\text{C NMR}$ (100 MHz, CDCl_3): δ 131.6, 128.2, 127.5, 124.1, 90.5, 80.6, 31.9, 29.7, 29.4, 29.2, 28.8, 22.7, 19.4, 14.2 ppm.



1-(Hex-1-yn-1-yl)-benzene (Table 5.1.4, entry 3): yellow liquid; $^1\text{H NMR}$ (400 MHz, CDCl_3): δ 7.40-7.38 (m, 2H), 7.27-7.25 (m, 3H), 2.41 (t, 2H, $J = 6.8$ Hz), 1.59-1.47 (m, 4H), 0.94 (t, 3H, $J = 7.3$ Hz) ppm. $^{13}\text{C NMR}$ (100 MHz, CDCl_3): δ 131.6, 128.2, 127.5, 124.1, 90.5, 80.6, 29.7, 22.1, 19.1, 13.7 ppm.

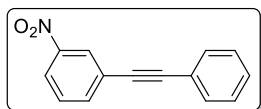


1-(Cyclohexylethynyl)benzene (Table 5.1.4, entry 4): Yellow liquid, $^1\text{H NMR}$ (400 MHz, CDCl_3): δ 7.45-7.38 (m, 1H), 7.33-7.32 (m, 1H), 7.27-7.25 (m, 3H), 2.60-2.56 (m, 1H), 1.77-1.25 (m, 10H) ppm. $^{13}\text{C NMR}$ (100 MHz, CDCl_3): δ 131.9, 131.6, 128.2, 127.4, 94.5, 80.5, 32.6, 29.7, 26.5, 24.9 ppm.



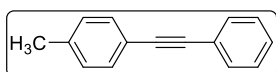
1-Nitro-4-(2-phenylethynyl)benzene (Table 5.1.4, entry 5): Yellow Solid, m.p. 119-121 °C, $^1\text{H NMR}$ (400 MHz, CDCl_3): δ

8.22 (d, 2H, $J = 8.8$ Hz), 7.68-7.66 (m, 2H), 7.57-7.55 (m, 2H), 7.40-7.38 (m, 3H) ppm. ^{13}C NMR (100 MHz, CDCl_3): δ 147.0, 132.3, 131.9, 130.3, 129.3, 128.6, 123.7, 122.1, 94.8, 87.6 ppm.



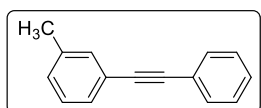
1-Nitro-3-(2-phenylethynyl)benzene (Table 5.1.4, entry 6):

Yellow gum, ^1H NMR (400 MHz, CDCl_3): δ 8.35 (s, 1H), 8.15 (d, 1H, $J = 8.2$ Hz), 7.80 (d, 1H, $J = 7.7$ Hz), 7.56-7.48 (m, 3H), 7.38-7.34 (m, 3H) ppm. ^{13}C NMR (100 MHz, CDCl_3): δ 148.2, 137.3, 131.8, 129.4, 129.1, 128.6, 126.4, 125.2, 122.9, 122.2, 92.0, 86.9 ppm.



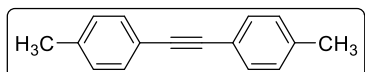
1-Methyl-4-(2-phenylethynyl)benzene (Table 5.1.4, entry 8,

17): White solid, m.p. 68-70 °C, ^1H NMR (400 MHz, CDCl_3): δ 7.56-7.50 (m, 2H), 7.42 (d, 2H, $J = 7.7$ Hz), 7.36-7.31 (m, 3H), 7.15 (d, 2H, $J = 7.7$ Hz), 2.36 (s, 3H) ppm. ^{13}C NMR (100 MHz, CDCl_3): δ 138.4, 132.6, 131.6, 131.2, 129.2, 128.4, 123.5, 120.2, 89.6, 88.8, 21.6 ppm.



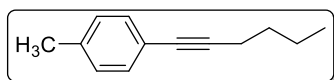
1-Methyl-3-(2-phenylethynyl)benzene (Table 5.1.4, entry 9):

Colourless liquid, ^1H NMR (400 MHz, CDCl_3): δ 7.53-7.51 (m, 2H), 7.36-7.33 (m, 4H), 7.25-7.21 (m, 2H), 7.14 (d, $J = 7.3$ Hz, 1H), 2.35 (s, 3H) ppm. ^{13}C NMR (100 MHz, CDCl_3): δ 138.1, 132.6, 131.7, 129.2, 128.4, 123.4, 123.1, 120.4, 89.6, 89.1, 21.3 ppm.



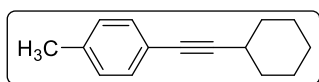
1-Methyl-4-[2-(*p*-tolyl)ethynyl]benzene (Table 5.1.4, entry 10), White solid, m.p. 126-128 °C, ^1H NMR (400

MHz, CDCl_3): δ 7.41 (d, 4H, $J = 8.0$ Hz), 7.14 (dd, 4H, $J = 7.9, 0.5$ Hz), 2.36 (s, 6H). ppm. ^{13}C NMR (100 MHz, CDCl_3): δ 138.2, 131.5, 129.3, 120.4, 88.9, 87.2, 21.5 ppm.



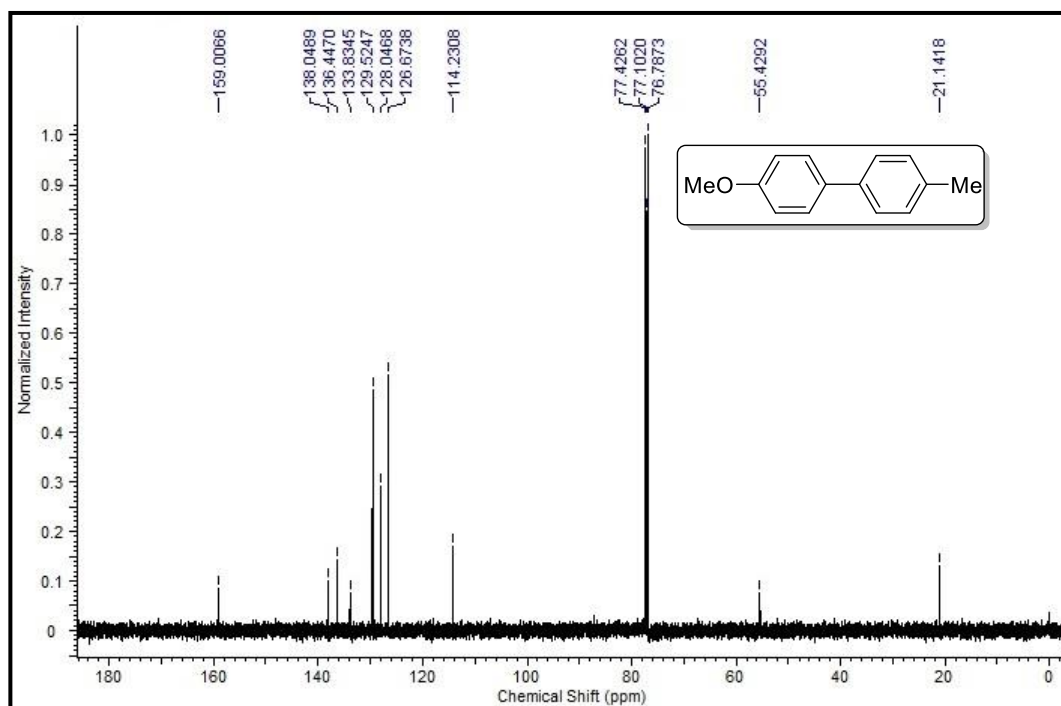
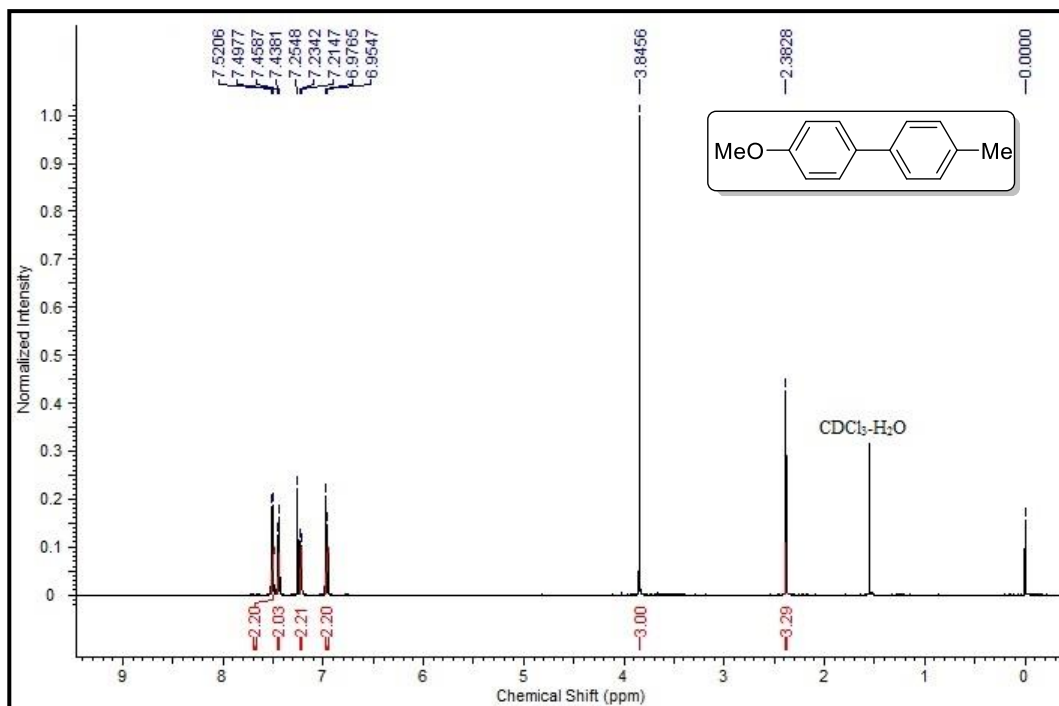
1-(Hex-1-yn-1-yl)-4-methylbenzene (Table 5.1.4, entry

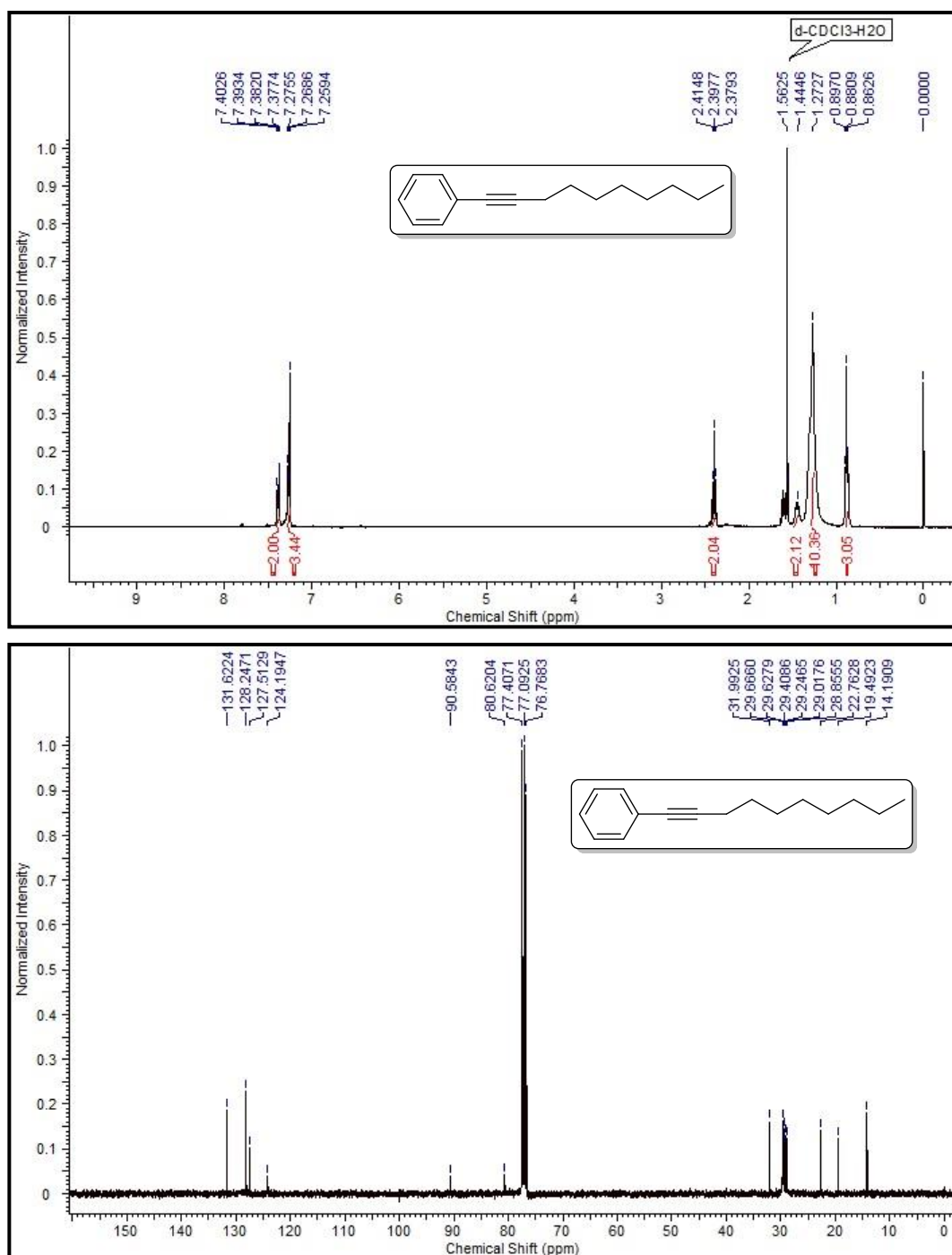
11), Yellow liquid, ^1H NMR (400 MHz, CDCl_3): δ 7.29-7.25 (m, 2H), 7.08-7.06 (m, 2H), 2.41-2.37 (m, 2H), 2.32 (s, 3H), 1.60-1.46 (m, 4H), 0.96-0.92 (m, 3H) ppm. ^{13}C NMR (100 MHz, CDCl_3): δ 137.4, 131.4, 129.3, 129.0, 128.0, 121.0, 89.6, 87.2, 30.9, 22.1, 21.4, 19.2, 13.7 ppm.



1-(Cyclohexylethynyl)-4-methylbenzene (Table 5.1.4, entry

12): Yellow liquid, ^1H NMR (400 MHz, CDCl_3): δ 7.29-7.10 (m, 4H), 2.58-2.56 (m, 1H), 2.37-2.32 (m, 3H), 1.73-1.26 (m, 10H) ppm. ^{13}C NMR (100 MHz, CDCl_3): δ 137.4, 131.8, 129.1, 128.8, 93.7, 80.6, 40.5, 32.8, 29.7, 26.0, 21.5 ppm.

^1H and ^{13}C NMR spectra of 4-Methyl-4'-methoxybiphenyl

^1H and ^{13}C NMR spectra of 1-(Dodec-1-yn-1-yl)-benzene

Section 5.2

Synthesis of copper NPs using papaya peel extract and its catalytic activity towards Sonogashira cross-coupling reaction

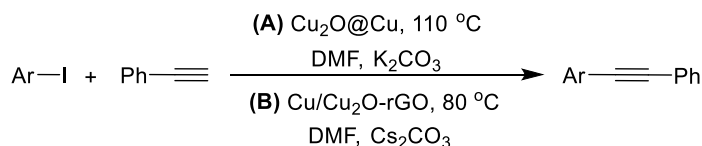
Abstract: In this section, a facile, inexpensive and eco-friendly method for synthesis of Cu₂O/Cu NPs has been developed using papaya peel extract. The copper NPs have been synthesized by hydrothermal method without the assistance of any reducing agents. The catalytic activity of the Cu₂O/Cu NPs was examined for palladium free Sonogashira type cross-coupling reaction of aryl iodides and phenylacetylenes.

5.2.1. Introduction

In the preceding section, agro-waste which in general is a significant source of pollution is effectively utilized as a biogenic medium for synthesis of palladium nanoparticles (Pd NPs). From various literature studies, we have come across that among all the transition metals, palladium is extensively used as a catalyst for various oxidative coupling reactions [1,2]. However, the economic threat of the present world leads the researchers to search for a simplified and economically viable catalytic protocol. Recently, focus has been made towards the synthesis of low cost metal NPs such as Ag [17], Cu [18], Ni [19] and Co [20]. However, synthesis of metal NPs requires external reducing sources or specific preparative mode which leads to environmental waste deposition with the release of toxic by-products. As such attention has been paid towards simple, safe and low cost alternative methodologies for synthesis of metal NPs.

As already discussed in the first chapter, the synthesis of diarylacetylenes was initially done in presence of copper [21]. However, the main issue arises in the case of product selectivity of the Sonogashira coupling due to involvement of terminal alkyne. So, careful modification regarding copper catalyst in association with various ligands assisting system for Sonogashira coupling have been reported [22]. But the ligand based system raises several drawbacks such as product isolation issues, stability, recyclability, cost and separate preparative methods. So, nowadays various approaches have been developed with the use of Cu NPs under reduced atmosphere for Sonogashira coupling reaction. Rothenberg *et al.* reported the first palladium-free and ligand-free Sonogashira cross-coupling, using heterogeneous copper nanoclusters as catalysts [23]. Later various Cu-based catalytic approaches have been made with the significant modification of catalytic system, temperature, solvent or other reaction parameters. For example, in 2012 Varma *et al.* developed a $\text{Cu}_2\text{O}@\text{Cu}$ composite and effectively utilized in Sonogashira coupling reaction of aryl iodides with phenyl acetylenes (Scheme 5.2.1A) [24]. Moreover, from the literature it is seen that Cu_2O NPs are highly active in Sonogashira coupling reaction. Recently, Gao and his co-workers reported a $\text{Cu}/\text{Cu}_2\text{O}$ NPs@graphene via “take” and “off” synthesis strategy with a Cu-MOF-derived jacket structure and described a synergistic effect between Cu(0) and Cu(I) that leads to an efficient catalysis for Sonogashira coupling (Scheme 5.2.1B) [25]. In view of this, we aimed to synthesize a two-phase one-pot $\text{Cu}_2\text{O}/\text{Cu}$ NPs using agro-waste (papaya peel extract) by simple hydrothermal treatment without the use of any additional basic medium or reducing

agent. The formation of the NPs was confirmed by solid UV, Powder XRD and FTIR analysis. The surface topology and porosity of the synthesized Cu₂O/Cu NPs was studied by SEM, TEM and BET surface analysis technique. The catalytic potential and the synergistic effect of Cu(0)-Cu(I) of the synthesized Cu₂O/Cu NPs was examined in palladium and ligand free Sonogashira coupling of aryl iodides and terminal alkynes.



Scheme 5.2.1: Sonogashira cross-coupling reaction using (A) Cu₂O@Cu composite (B) Cu/Cu₂O-rGO with a Cu-MOF-derived jacket structure.

5.2.2. Experimental

5.2.2.1. General procedure for preparation of Cu₂O/Cu NPs

Papaya peel (10 g) was washed with distilled water, finely chopped and then grinded with 100 mL distilled water. The extract was filtered through sintered glass crucible. In a 100 mL teflon-lined stainless steel autoclave, 0.5 g Cu(OAc)₂ was mixed with 40 mL papaya peel extract. The mixture was allowed to stir for 30 minutes to obtain a homogeneous solution of Cu(OAc)₂. Thereafter the resulting mixture was sealed and subjected to heating at 160°C for 7h. In a similar procedure, another mixture was prepared and subjected to heating at 190°C. Hydrothermal heating of Cu(OAc)₂/papaya peel extract mixture at 160°C (Cu-433K) produced reddish brown precipitate whereas brownish black precipitate was obtained at 190°C (Cu-463K). The resulting residue (NPs) was separated by centrifugation, washed with distilled water and ethanol and dried in vacuum for further analytical experiments (Figure 5.2.1).

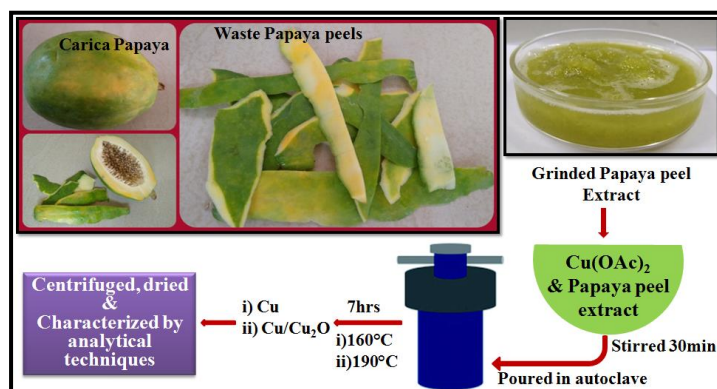


Figure 5.2.1: Preparation of Cu NPs using papaya peel extract.

5.2.2.2. General procedure for Sonogashira cross-coupling reactions

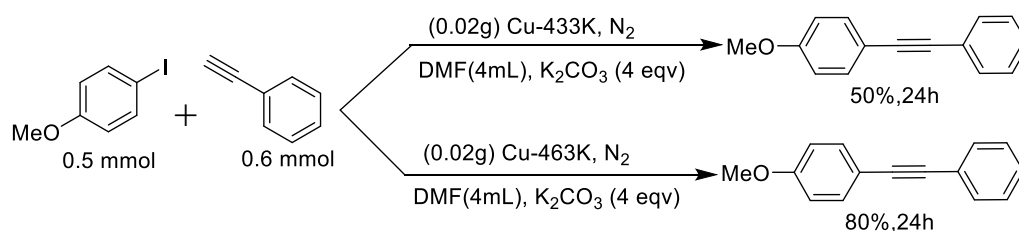
In a 100 mL two-necked round-bottom flask, aryl iodides (1 mmol), terminal acetylene (1.2 mmol), base (2 mmol) and copper NPs (10 wt%) were mixed in DMF (4 mL). The reaction mixture was sealed with rubber septum and subjected to stirring. Subsequently, the air inside the round bottom flask was replaced with nitrogen (balloon) by three vacuum/nitrogen cycles. After completion (vide TLC) the catalyst was separated from the reaction mixture by centrifugation and the crude reaction mixture was extracted with ethyl acetate (3×10 mL) and dried over anhydrous Na₂SO₄. The products were purified by column chromatography using n-hexane and ethyl acetate as eluent. The products were identified by ¹H and ¹³C NMR spectroscopic analyses.

For recycling experiments, the reaction mixture was centrifuged and the residue catalyst was washed four times with excess water and then with ethyl acetate in sequence. The resultant catalyst was dried under vacuum and subjected to further catalytic run.

5.2.3. Results and Discussion

5.2.3.1. Controlled experiment using both the synthesised copper NPs

Initially, the catalytic activities of the copper nanoparticles were investigated for Sonogashira cross-coupling reaction considering 4-iodoanisole and phenylacetylene as the model substrate. The reaction was performed under N₂ atmosphere using K₂CO₃ as base in DMF as the reaction medium. A significant difference in catalytic activity for both the copper nanoparticles was observed with Cu-463K being more competent than Cu-433K (Scheme 5.2.2).



Scheme 5.2.2: Controlled experiment for Sonogashira cross-coupling using Cu-433K and Cu-463K.

5.2.3.2. Characterizations of the synthesised copper NPs

Initially, in order to confirm the reduction of Cu(II) species, we have performed solid state UV/Vis spectroscopic experiment. The difference in absorbance of the synthesized

copper NPs from the precursor $\text{Cu}(\text{OAc})_2$, reveals the reduction of $\text{Cu}(\text{II})$ ion (Figure 5.2.2a). In order to reveal the difference in reactivity of both the catalyst, initially we have performed the powder XRD analysis for both the copper NPs (Cu-433K and Cu-463K) (Figure 5.2.2b). The powder XRD pattern for Cu-433K is identical to that of pure Cu with cubic fcc structure (JCPDS- 85-1326). The diffraction pattern is observed at 2θ values 43.2, 50.3 and 74.1 corresponding to crystal planes (111) (200) and (220) with lattice parameter $a=3.615$. The sharp peaks indicate its highly crystalline nature with no other impurities. A slight difference in XRD pattern of Cu-463K was observed with an additional weak peak at 2θ value of 36.4 with the reflection of (111) plane of cubic Cu_2O nanostructure (JCPDS-78-2076). The diffraction peaks ascribed due to Cu_2O is due to the *in situ* transformation of Cu to Cu_2O on increasing the temperature. This is because, pure Cu does not react with water but, instead it reacts with steam to give hydrogen gas and metal oxides. So, on being subjected to high temperature, the oxidation of Cu occurs with increasing water vapour pressure due to the increased copper vacancy. As such at $190\text{ }^\circ\text{C}$, most of the water molecules are in their vapour state and leads to oxidation of some $\text{Cu}(0)$ species to Cu_2O [26].

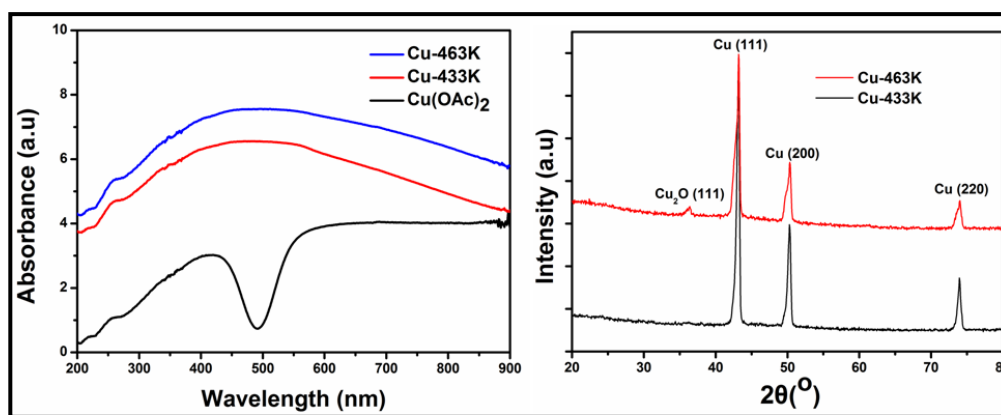


Figure 5.2.2: (a) Solid state UV/Vis spectra of $\text{Cu}(\text{OAc})_2$, Cu-433K and Cu-463K (b) Powder XRD pattern of Cu-433K and Cu-463K.

From the controlled experiment for Sonogashira coupling (Scheme 5.2.1), we have found that Cu-463K provide greater catalytic activity. This is due to the *in situ* formation of Cu_2O , which results in a synergistic interaction between $\text{Cu}(0)$ and $\text{Cu}(\text{I})$ ion, leading to greater catalytic activity in the coupling reaction [25]. So, as per the catalytic efficiency and in order to study the nature of Cu-463K i.e. $\text{Cu}_2\text{O}/\text{Cu}$ NPs, further characterizations regarding composition, surface area/morphology has been done using Cu-463K. FTIR spectrum of the $\text{Cu}(\text{OAc})_2$ and Cu-463K were recorded (Figure 5.2.3 a

and b). The diminished vibrational modes due to absence of metal-ligand interaction in the region of $1000\text{-}500\text{ cm}^{-1}$ for Cu-463K signifies the decomposition of Cu(II) species. Energy dispersive X-ray (EDX) analysis of the Cu-463K reveals the presence of Cu and O with devoid of any other impurities (Figure 5.2.3c).

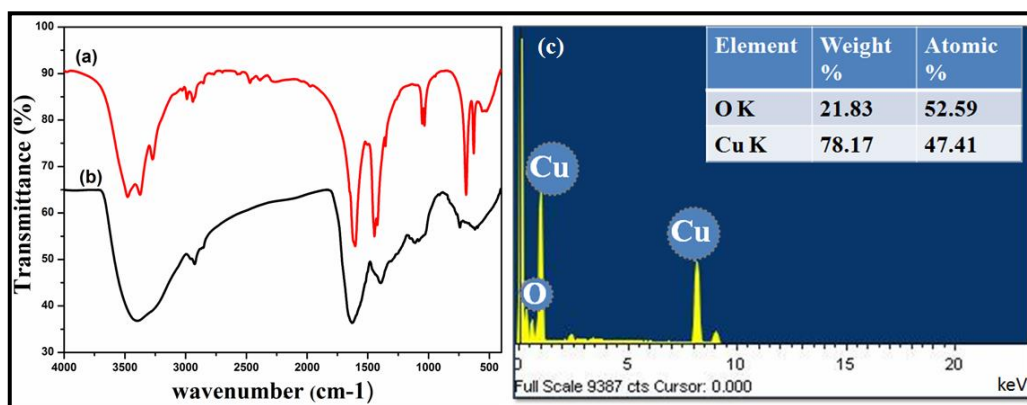


Figure 5.2.3: FTIR spectra of (a) $\text{Cu}(\text{OAc})_2$ and (b) Cu-463K NP (c) EDX analysis of Cu-463K NP.

The morphology of the Cu-463K was studied by TEM imaging. From the TEM images, two different Cu phases can be distinguish which represents Cu(0) and Cu_2O particles (Figure 5.2.4 a, b and c).

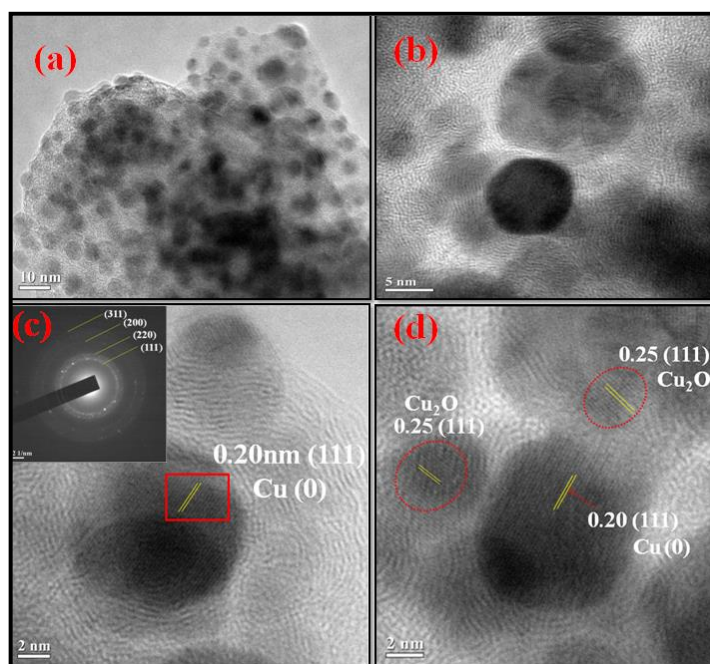


Figure 5.2.4: (a, b, c and d) are the TEM and HRTEM images and inset in (c) is the SAED pattern of the Cu-463K NPs.

Both the copper phases and particles are distributed like a lamellar sheet stacked one above the other (Figure 5.2.4 a-c). From the HRTEM images, the two phases could be distinguished which showed lattice fringes with an interlayer spacing of 0.20 nm and 0.25 nm due to the (111) lattice plane of Cu and Cu₂O respectively (Figure 5.2.4 d). Moreover the inset in Figure 5.2.4c, represents the SAED pattern with four well resolved rings corresponding to (111), (220), (200) and (311) reflection of face centered cubic (fcc) Cu NPs.

Further the surface characteristic of the Cu-463K NPs was identified by scanning electron microscopy (SEM) images (Figure 5.2.5 a, b and c). It can be seen that the smaller particles of Cu₂O are stacked above the spherical Cu(0) NPs. Moreover, from Figure 5.2.5 b and c, it is seen that Cu₂O/Cu NPs surface is porous in nature.

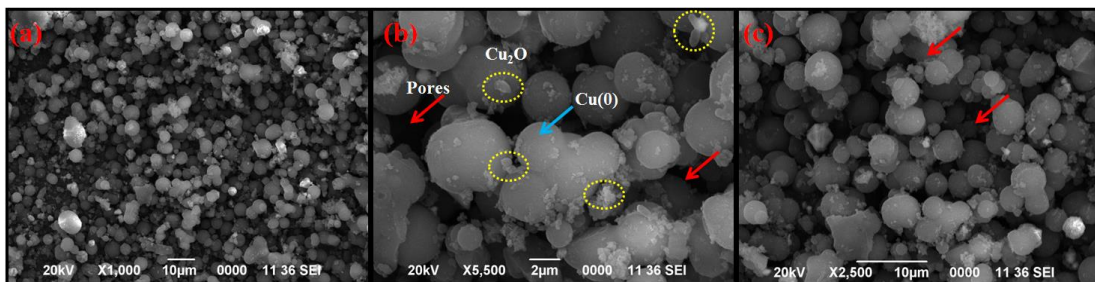


Figure 5.2.5: (a, b, and c) are the SEM images of Cu-463K.

Next, in order to examine the porous behaviour and to evaluate the surface area and pore size distribution of Cu-463K, BET surface analysis technique was employed (Figure 5.2.6).

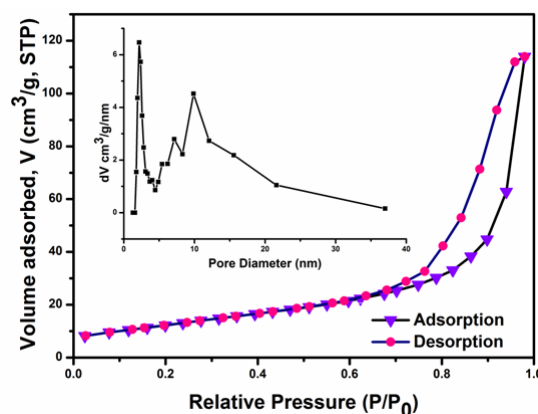


Figure 5.2.6: BET surface area and pore size distribution (inset) of Cu-463K.

From the nitrogen adsorption-desorption (BET) experiment, it was found that the curve belonged to the type IV isotherm with distinct H3 hysteresis loops. Hysteresis above $P/P_0 \sim 0.6$ (N_2 @77K) is due to the presence of the mesopores. Further, surface area of the Cu-463K NPs as calculated by the BET equation was about $45.249 \text{ m}^2/\text{g}$ with pore volume $0.176 \text{ cm}^3/\text{g}$ and an average BJH pore diameter of 9.864 nm . Moreover, the pore size distribution curve (inset) also indicates the mesoporosity of the $\text{Cu}_2\text{O}/\text{Cu}$ NPs (Cu-463K).

5.2.3.3. Catalytic activity of the $\text{Cu}_2\text{O}/\text{Cu}$ NPs (Cu-463K)

5.2.3.3.1. Optimization of catalytic system for Sonogashira coupling reaction

The efficiency of $\text{Cu}_2\text{O}/\text{Cu}$ NPs (Cu-463K) was examined in Sonogashira coupling reaction considering different reaction parameter. For the purpose 4-iodonitrobenzene and phenylacetylene was employed as a model substrates using Cu-463K (20 wt%) and the reaction was studied by varying the solvent system, catalyst loading, bases and temperature (Table 5.1.1). Among the different solvents, DMF serve to be an excellent reaction medium for the cross-coupling reaction (Table 5.1.1, entries 1-5). This may be because DMF stabilized the $\text{Cu}_2\text{O}/\text{Cu}$ NPs (Cu-463K) in solution phase and assists in providing better catalytic performance [27]. Since the reaction was initially performed with 20 wt% Cu-463K, we than tried to lower the amount of catalyst loading (Table 5.1.1, entries 6-8). Interestingly, the reaction proceeds well in minimizing the catalyst amount to 10 wt% (Table 5.1.1, entry 7). Next the effect of different bases was studied for this catalytic system, carbonates of potassium and cesium provides better efficiency and carbonate and hydroxide of sodium deliver only trace amount of conversion (Table 5.1.1, entries 9-11). However, K_2CO_3 was found to be the most effective in terms of reaction efficiency and time (Table 5.1.1, entries 7 vs 9-11). The activity of the catalytic system was also studied by lowering the temperature but lower yield of diarylalkyne was obtained (Table 5.1.1, entry 12). Generally, in order to avoid dimerization of terminal alkyne, the copper catalyzed Sonogashira coupling was performed under reduced atmosphere. But in order to verify this we have performed the reaction in aerobic condition. The reaction yield significantly decreases in presence of air (Table 5.1.1, entry 13).

Table 5.2.1: Optimization of catalytic system for Sonogashira cross-coupling reaction ^[a]

Entry	Cu-463K (wt %)	Base (mmol)	Solvent (mL)	Temp. (°C)	Time (h)	Yield (%) ^[b]
1	20	K ₂ CO ₃	Water	90	24	20
2	20	K ₂ CO ₃	EtOH	80	24	50
3	20	K ₂ CO ₃	1,4-Dioxane	90	24	nr
4	20	K ₂ CO ₃	EtOH/H ₂ O(1:1)	90	24	40
5	20	K ₂ CO ₃	DMF	90	12	92
6	5	K ₂ CO ₃	DMF	90	24	40
7	10	K ₂ CO ₃	DMF	90	12	90
8	15	K ₂ CO ₃	DMF	90	12	90
9	10	Cs ₂ CO ₃	DMF	90	12	88
10	10	Na ₂ CO ₃	DMF	90	24	Trace
11	10	NaOH	DMF	90	24	Trace
12	10	K ₂ CO ₃	DMF	60	24	40
13	10	K ₂ CO ₃	DMF	90	12	75 ^[c]

^[a] Reaction conditions: 4-iodonitrobenzene (0.5 mmol), phenylacetylene (0.6 mmol), Base (2 mmol), Solvent (4 mL), N₂ atm ^[b] Isolated yield ^[c] in air

5.2.3.3.2. Substrate scope for Sonogashira coupling reaction

Considering the optimized condition from Table 5.2.1, the activity of Cu-463K was studied for Sonogashira coupling of electronically diverse aryl iodides and phenylacetylene (Table 5.2.2). The reaction provides excellent conversion for *para*- and *meta*- substituted electron withdrawing aryl iodides (Table 5.2.2, entries 1-8). However, catalytic activity seems to be moderate for 4-bromoiodobenzene (Table 5.2.2, entry 3). This may be due to the contribution of positive resonance effect (+R) of the bromo substituent which increases the electron density over phenyl ring and causes difficulty in C-I bond breaking. Again, it is observed that electron donating aryl iodides are less competent than electron withdrawing species (Table 5.2.2, entry 4). Next the effect of different substituted phenylacetylene was studied and no such significant difference in yield and duration on the cross-coupling reaction was observed (Table 5.2.2, entries 7 and 8). It was found that coupling of 3-iodobenzaldehyde and 3-methylphenylacetylene results in poor conversion (Table 5.2.2, entry 9). Again, the coupling of heteroaryl iodide for example, 3-iodopyridine was investigated, and moderate yield of cross-coupling product was obtained (Table 5.2.2, entry 10).

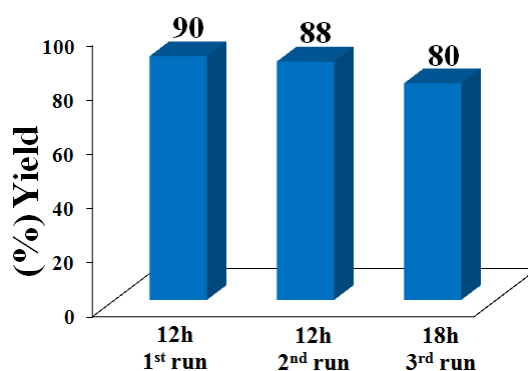
Table 5.2.2: Sonogashira cross-coupling of aryl iodides and phenylacetylene ^[a]

Entry	R ¹	R ²	Time(h)	Yield (%) ^[b]
1	4-NO ₂	C ₆ H ₅	12	90
2	4-COMe	C ₆ H ₅	12	91
3	4-Br	C ₆ H ₅	24	70
4	4-OMe	C ₆ H ₅	24	80
5	3-NO ₂	C ₆ H ₅	12	85
6	3-CHO	C ₆ H ₅	24	80
7	4-NO ₂	4-MeC ₆ H ₅	12	90
8	4-COMe	3-MeC ₆ H ₅	24	80
9	3-CHO	3-MeC ₆ H ₅	24	40
10	3-Iodopyridine	C ₆ H ₅	12	60

^[a] Reaction conditions: aryl iodide (0.5mmol), phenylacetylene (0.6 mmol), K₂CO₃ (2 mmol), Cu-463K (10wt%), DMF (4 mL), N₂ atm; ^[b] Isolated yield

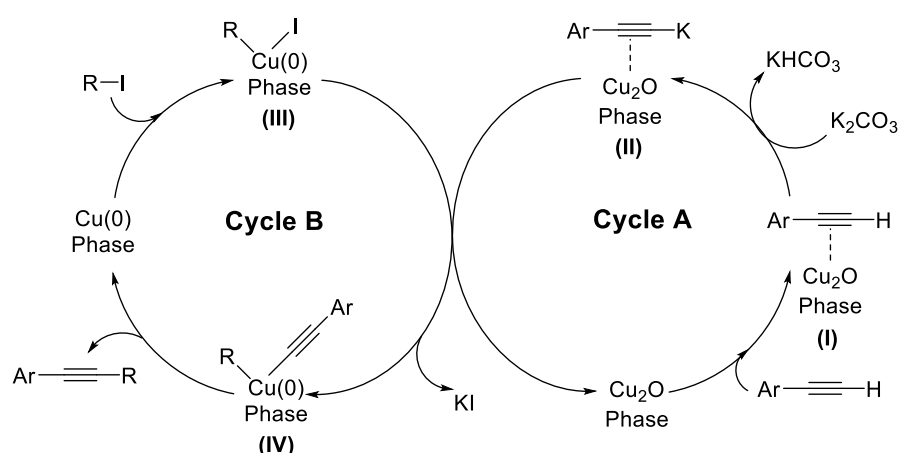
5.2.3.4. Catalyst reusability

The recyclability of the Cu-463K was investigated using 4-iodonitrobenzene and phenylacetylene using the optimized reaction condition (Figure 5.2.7). After the fresh catalytic run, the reaction mixture was subjected to centrifugation and the residue catalyst was washed with excess water and ethyl acetate in sequence which is then dried under vacuum. Thereafter, the catalyst was used for next consecutive run with the addition of fresh reactants, base and solvent. We have observed that the catalyst can be effectively reused up to third catalytic cycles without significant loss in its catalytic activity.

**Figure 5.2.7:** Reusability of Cu-463K in Sonogashira cross-coupling reaction.

5.2.3.5. Study of synergistic action of Cu₂O/Cu in Sonogashira coupling reaction

Gao and Zheng recently reported a Cu/Cu₂O NPs@graphene via “take” and “off” synthesis strategy with a Cu-MOF-derived jacket structure [25]. They proposed a mechanistic pathway in which a synergistic interaction of the Cu and Cu₂O phase was described which assists in the efficient catalysis of the Sonogashira cross-coupling reaction. Based on this, similar effect might be present in our current protocol with Cu(0) and Cu₂O particles leading to a synergistic effect in the coupling of aryl halide and terminal alkyne (Scheme 5.2.3). This was also evidenced by the controlled experiment mentioned in Scheme 5.2.2, where Cu(0) NPs doesn't provide efficient coupling. This proves that the presence of Cu₂O has a remarkable effect in the coupling reaction. As discussed by Lan and Lei, Cu(I) has a stronger interaction with alkyne and increases the acidity of the inactive C–H bond [28]. The alkyne carbanion formed as result of deprotonation of the terminal alkyne coordinates with base to form an active intermediate (II). Consequently, the copper phase assists in the oxidative addition of aryl iodide which then undergoes transmetalation to form aryl copper acetylide intermediate (IV). Reductive elimination of the species results the diarylalkyne with the regeneration of the catalytic species. As per literature, the coordination of Cu(I) species with alkyne is proved to be a fast step in the reaction [28]. However, the efficient contribution of both the copper phase in the catalytic cycle proves that the reaction proceeds with the synergistic association of Cu phase and Cu₂O phase.

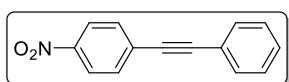


Scheme 5.2.3: Plausible mechanistic action of Cu/Cu₂O NPs in Sonogashira coupling reaction.

5.2.4. Conclusions

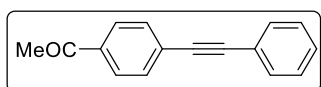
In summary, the present methodology provides a green and economical alternative strategy for palladium and ligand free Sonogashira coupling reaction using an agro-waste extract. The synthesis of catalytic species involves a one pot green condition without the assistance of conventional chemicals. Moreover a two phase catalytic species is formed which results in a synergistic effect for the efficient C-C coupling reaction.

5.2.5. Analytical data of the synthesized alkynyl derivatives



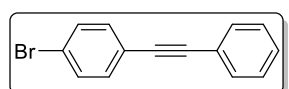
1-Nitro-4-(2-phenylethynyl)benzene (Table 5.2.2, entry 1):

Yellow Solid, $^1\text{H NMR}$ (400 MHz, CDCl_3): δ 8.26-8.16 (m, 2H), 7.69-7.62 (m, 2H), 7.55 (ddd, 2H, $J = 6.1, 3.7, 1.2$ Hz), 7.43-7.33 (m, 3H).ppm. $^{13}\text{C NMR}$ (100 MHz, CDCl_3): δ 147.0, 132.3, 131.9, 130.3, 129.3, 128.6, 123.7, 122.1, 94.8, 87.6 ppm.



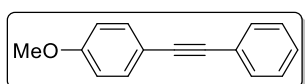
1-Acetyl-4-(2-phenylethynyl)benzene (Table 5.2.2, entry 2):

White Solid, $^1\text{H NMR}$ (400 MHz, CDCl_3): δ 7.97-7.88 (m, 2H), 7.65-7.58 (m, 2H), 7.57-7.50 (m, 2H), 7.39-7.32 (m, 3H), 2.60 (s, 3H).ppm. $^{13}\text{C NMR}$ (100 MHz, CDCl_3): δ 197.4, 136.2, 131.8, 131.7, 128.9, 128.5, 128.3, 128.2, 122.7, 92.7, 88.6, 26.7 ppm.



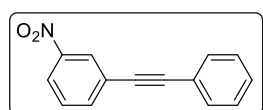
1-Bromo-4-(2-phenylethynyl)benzene (Table 5.2.2, entry 3):

White Solid, $^1\text{H NMR}$ (400 MHz, CDCl_3): δ 7.55-7.47 (m, 4H), 7.36-7.30 (m, 5H).ppm. $^{13}\text{C NMR}$ (100 MHz, CDCl_3): δ 132.5, 129.3, 128.5, 121.8, 99.9, 92.6 ppm.



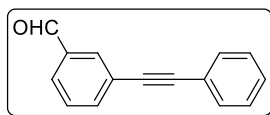
1-Methoxy-4-(2-phenylethynyl)benzene (Table 5.2.2, entry

4): White Solid, $^1\text{H NMR}$ (400 MHz, CDCl_3): δ 7.49 (dd, 4H, $J = 15.8, 7.4$ Hz), 7.30 (t, 3H, $J = 17.3$ Hz), 6.88 (d, 2H, $J = 8.6$ Hz), 3.82 (s, 3H).ppm. $^{13}\text{C NMR}$ (100 MHz, CDCl_3): δ 159.6, 133.1, 131.5, 128.4, 128.0, 123.6, 115.4, 114.0, 89.4, 87.2, 55.3 ppm.



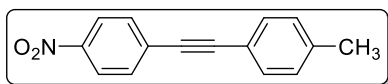
1-Nitro-3-(2-phenylethynyl)benzene (Table 5.2.2, entry 5):

Yellow gum, $^1\text{H NMR}$ (400 MHz, CDCl_3): δ 8.35 (s, 1H), 8.22-8.09 (m, 1H), 7.80 (dd, 1H, $J = 7.7, 1.1$ Hz), 7.60-7.45 (m, 3H), 7.43-7.28 (m, 3H).ppm. $^{13}\text{C NMR}$ (100 MHz, CDCl_3): δ 148.2, 137.3, 131.9, 129.5, 129.1, 128.6, 126.4, 125.2, 122.9, 122.2, 92.0, 86.9 ppm.



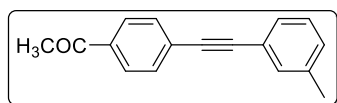
1-Formyl-3-(2-phenylethynyl)benzene (Table 5.2.2, entry 6):

Yellow gum, $^1\text{H NMR}$ (400 MHz, CDCl_3): δ 10.01 (s, 1H), 8.02 (td, 1H, $J = 1.6, 0.5$ Hz), 7.85-7.72 (m, 2H), 7.58-7.48 (m, 3H), 7.40-7.29 (m, 3H).ppm. $^{13}\text{C NMR}$ (100 MHz, CDCl_3): δ 191.6, 137.2, 136.5, 133.0, 131.7, 129.2, 128.9, 128.8, 128.5, 124.6, 122.7, 91.0, 87.9 ppm.



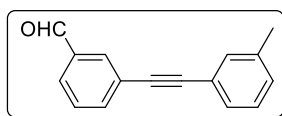
1-Methyl-4-[2-(4-nitrophenyl)ethynyl]benzene (Table

5.2.2, entry 7): Light yellow solid, $^1\text{H NMR}$ (400 MHz, CDCl_3): δ 8.33-8.03 (m, 2H), 7.70-7.54 (m, 2H), 7.44 (d, 2H, $J = 8.0$ Hz), 7.18 (d, 2H, $J = 7.9$ Hz), 2.38 (s, 3H) ppm. $^{13}\text{C NMR}$ (100 MHz, CDCl_3): δ 146.9, 139.7, 132.3, 131.8, 130.6, 129.4, 123.7, 119.1, 95.1, 87.1, 21.6 ppm.



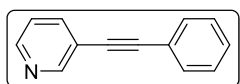
1-Acetyl-4-[2-(3-methylphenyl)ethynyl]benzene (Table

5.2.2, entry 8): White solid, $^1\text{H NMR}$ (400 MHz, CDCl_3): δ 7.99-7.85 (m, 2H), 7.63-7.52 (m, 2H), 7.43 (d, 2H, $J = 8.1$ Hz), 7.16 (d, 2H, $J = 7.9$ Hz), 2.60 (s, 3H), 2.37 (s, 3H).ppm. $^{13}\text{C NMR}$ (100 MHz, CDCl_3): δ 197.4, 139.1, 136.1, 131.7, 131.6, 129.3, 128.5, 128.4, 128.3, 119.6, 93.1, 88.1, 26.7, 21.6 ppm.



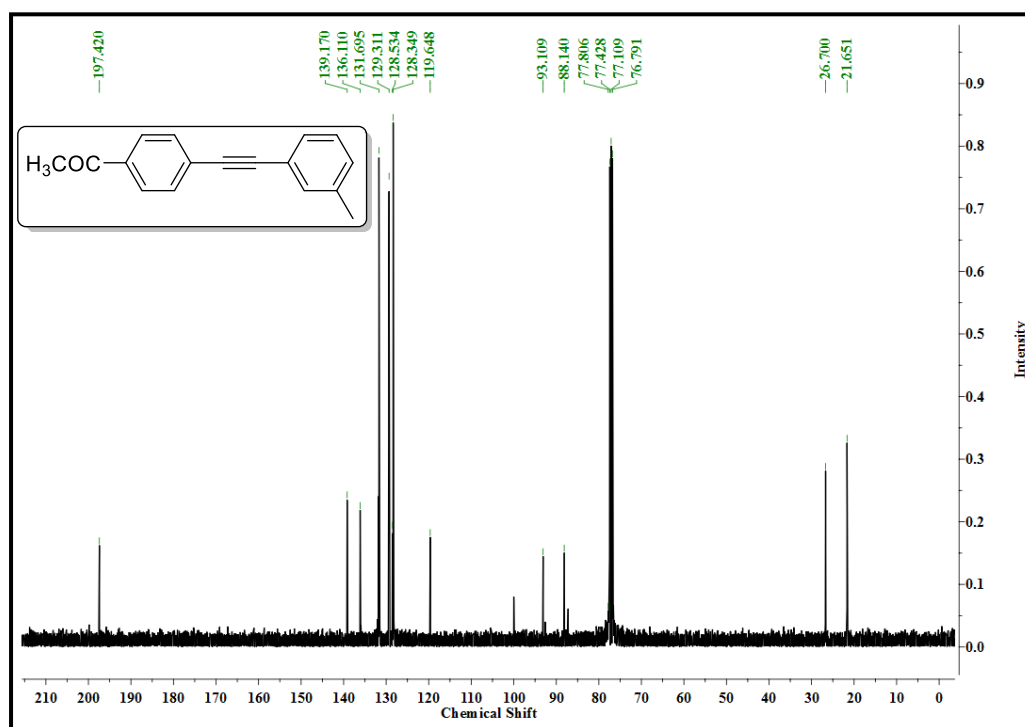
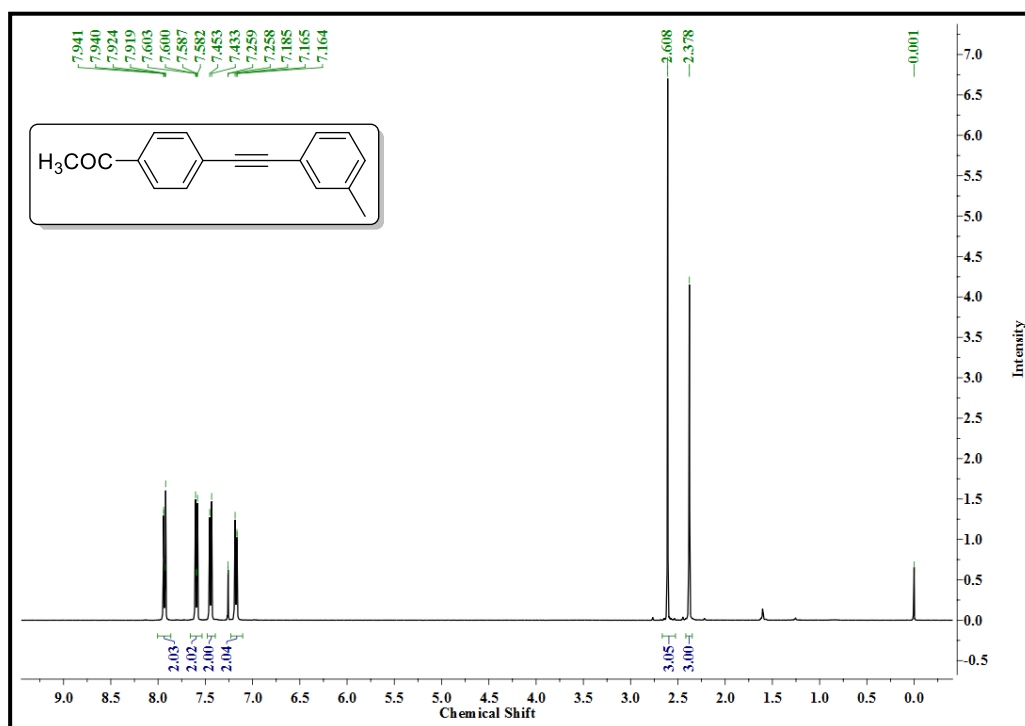
1-Formyl-3-[2-(3-methylphenyl)ethynyl]benzene (Table

5.2.2, entry 9): Yellow gum, $^1\text{H NMR}$ (400 MHz, CDCl_3): δ 10.01 (s, 1H), 8.27-8.01 (m, 4H), 7.85-7.16 (m, 4H) ppm. $^{13}\text{C NMR}$ (100 MHz, CDCl_3): δ 191.6, 170.3, 138.2, 129.7, 129.5, 129.1, 128.8, 128.6, 128.4, 128.3, 124.7, 124.1, 122.5, 99.9, 87.5, 21.2 ppm.



3-(Phenylethynyl)pyridine (Table 5.2.2, entry 10): Yellow liquid,

$^1\text{H NMR}$ (400 MHz, CDCl_3): δ 8.79-8.78 (m, 1H), 8.56 (dd, 1H, $J = 4.9, 1.7$ Hz), 7.87-7.78 (m, 1H), 7.60-7.48 (m, 2H), 7.43-7.23 (m, 4H).ppm. $^{13}\text{C NMR}$ (100 MHz, CDCl_3): δ 152.2, 148.5, 138.4, 131.7, 131.6, 128.8, 128.4, 123.0, 122.4, 92.6, 85.9 ppm.

^1H and ^{13}C NMR spectra of 1-Acetyl-4-[2-(3-methylphenyl)ethynyl]benzene

5.3. References

- [1] Nicolaou, C. K., Bulger, G. P., and Sarlah, D. Palladium-catalyzed cross-coupling reactions in total synthesis. *Angewandte Chemie International Edition*, 44(29):4442-4489, 2005.
- [2] Sellars, J. D. and Steel, P. G. Transition metal-catalyzed cross-coupling reactions of P-activated enols. *Chemical Society Reviews*, 40(10):5170-5180, 2011.
- [3] Mazur, M. Electrochemically prepared silver nanoflakes and nanowires. *Electrochemistry Communications*, 6(4):400-403, 2004.
- [4] Shankar, S. S., Rai, A., Ahmad, A., and Sastry, M. Rapid synthesis of Au, Ag, and bimetallic Au Core-Ag shell nanoparticles using neem (*Azadirachta Indica*) leaf broth. *Journal of Colloid and Interface Science*, 275(2):496-502, 2004.
- [5] Kharissova, V. O., Dias, R. V. H., Kharisov, I. B., Perez, O. B., and Perez, J. M. V. Greener synthesis of nanoparticles. *Trends in Biotechnology*, 31(4):240-248, 2013.
- [6] Rudra, G. S., Nishad, J., Jakhar, N., and Kaur, C. Food industry waste: Mine of nutraceuticals. *International Journal of Science, Environment and Technology*, 4(1):205-229, 2015.
- [7] De Melo, M. E., Clark, H. J., and Matharu, S. A. The Hy-MASS concept: Hydrothermal microwave assisted selective scissoring of cellulose for insitu production of (meso)porous nanocellulose fibrils and crystals. *Green Chemistry*, 19(14):3408-3417, 2017.
- [8] Pelissari, M. F., Sobral, A. J. P., and Menegalli, C. F. Isolation and characterization of cellulose nanofibers from banana peels. *Cellulose*, 21(1):417-432, 2014.
- [9] Balavijayalakshmi, J. and Ramalakshmi, V. Carica Papaya peel mediated synthesis of silver nanoparticles and its antibacterial activity against human pathogens. *Journal of Applied Research and Technology*, 15(5):413-422, 2017.
- [10] Kalaiselvi, A., Roopan, M. S., Madhumitha, G., Ramalingam, C., and Elango, G. Synthesis and characterization of palladium nanoparticles using *Catharanthus roseus* leaf extract and its application in the photo-catalytic degradation. *Spectrochimica Acta Part A: Molecular and Biomolecular Spectroscopy*, 135:116-119, 2015.
- [11] Yang, X., Li, Q., Wang, H., Huang, J., Lin, L., Wang, W., Sun, D., Su, Y., Opiyo, B. J., Hong, L., Wang, Y., He, N., and Jia, L. Green synthesis of palladium nanoparticles using broth of *Cinnamomum camphora* leaf. *Journal of Nanoparticle Research*, 12(5):1589-1598, 2010.

- [12] Dewan, A., Bharali, P., Bora, U., and Thakur, J. A. Starch assisted palladium(0) nanoparticles as in situ generated catalysts for room temperature Suzuki-Miyaura reaction in water. *RSC Advances*, 6(14):11758-11762, 2016.
- [13] Boruah, P. R., Ali, A. A., Saikia, B., and Sarma, D. A novel green protocol for ligand free suzuki-miyaura cross-coupling reactions in WEB at room temperature. *Green Chemistry*, 17(3):1442-1445, 2015.
- [14] Bhaskar, R., Sharma, A. K., Yadav, M. K., and Singh, A. K. Sonogashira (Cu and amine free) and Suzuki coupling in air catalyzed via nanoparticles formed in situ from Pd(II) complexes of chalcogenated Schiff bases of 1-naphthaldehyde and their reduced forms. *Dalton Transction*, 46(44):15235-15248, 2017.
- [15] Mikhaylov, V. N., Sorokoumov, V. N., Korvinson, K. A., Novikov, A. S., and Balova, I. A. Synthesis and simple immobilization of palladium(II) acyclic diaminocarbene complexes on polystyrene support as efficient catalysts for Sonogashira and Suzuki-Miyaura cross-coupling. *Organometallics*, 35(11):1684-1697, 2016.
- [16] Li, P., Wang, L., Zhang, L., and Wang, G.-W. Magnetic nanoparticles-supported palladium: A highly efficient and reusable catalyst for the Suzuki, Sonogashira, and Heck reactions, *Advanced Synthesis & Catalysis*, 354(7):1307-1318, 2012.
- [17] Das, V. K., Harsh, S. N., and Karak, N. Highly efficient and active silver nanoparticle catalyzed conversion of aldehydes into nitriles: A greener, convenient, and versatile 'NOSE' approach. *Tetrahedron Letters*, 57(5):549-553, 2016.
- [18] Gawande, M. B., Goswami, A., Felpin, F. X., Asefa, T., Huang, X., Silva, R., Zou, X., Zboril, R., and Varma, R. S., Cu and Cu-based nanoparticles: Synthesis and applications in catalysis. *Chemical Reviews*, 116(6):3722-3811, 2016.
- [19] Sengupta, D., Bhowmik, K., De, G., and Basu, B. Ni Nanoparticles on rGO as reusable heterogeneous catalyst: Effect of Ni particle size and intermediate composite structures in C-S cross-coupling reaction. *Beilstein Journal of Organic Chemistry*, 13:1796-1806, 2017.
- [20] Zhang, L., Wang, A., Wang, W., Huang, Y., Liu, X., Miao, S., Liu, J., and Zhang, T., Co-N-C catalyst for C-C coupling reactions: On the catalytic performance and active sites. *ACS Catalysis*, 5(11):6563-6572, 2015.

- [21] Stephens, R. D. and Castro, C. E. The substitution of aryl iodides with cuprous acetylides. A synthesis of tolans and heterocyclics. *The Journal of Organic Chemistry*, 28(12):3313-3315, 1963.
- [22] Thomas, A. M., Sujatha, A., and Anilkumar, G. Recent advances and perspectives in copper-catalyzed sonogashira coupling reactions. *RSC Advances*, 4(42):21688-21698, 2014.
- [23] Thathagar, M. B., Beckers, J., and Rothenberg, G. Palladium-free and ligand-free Sonogashira cross-coupling. *Green Chemistry*, 6(4):215-218, 2004.
- [24] Kou, J., Saha, A., Bennett-Stamper, C., and Varma, R. S. Inside-out core-shell architecture: Controllable fabrication of Cu₂O@Cu with high activity for the Sonogashira coupling reaction. *Chemical Communications*, 48(47):5862-5864, 2012.
- [25] Sun, W., Gao, L., Sun, X., and Zheng, G. A novel route with a Cu (II)-MOF-derived structure to synthesize Cu/Cu₂O NPs@ graphene: The electron transfer leads to the synergistic effect of the Cu(0)-Cu(I) phase for an effective catalysis of the Sonogashira cross-coupling reactions. *Dalton Transactions*, 47(16):5538-5541, 2018.
- [26] Wang, J. P. and WD, C. Oxidation behavior of pure copper in oxygen and/or water vapor at intermediate temperature. *ISIJ International*, 49(12):1926-1931, 2009.
- [27] Oka, H., Kitai, K., Suzuki, T., and Obora, Y. N, N-Dimethylformamide-stabilized copper nanoparticles as a catalyst precursor for Sonogashira-Hagihara cross coupling. *rsc advances*, 7(37):22869-22874, 2017.
- [28] Bai, R., Zhang, G., Yi, H., Huang, Z., Qi, X., Liu, C., and Lei, A. Cu(II)-Cu(I) synergistic cooperation to lead the alkyne C-H activation. *Journal of the American Chemical Society*, 136(48):16760-16763, 2014.